A *Drosophila* Model of Pontocerebellar Hypoplasia Reveals a Critical Role for the RNA Exosome in Neurons

Derrick J. Morton[1,2,6], Binta Jalloh[3,4], Lily Kim[1], Isaac Kremsky[1], Thaila Le[1], Khuong B. Nguyen[1], J. Christopher Rounds[3,4], Maria C. Sterrett[1,5], Brianna Brown[4], Sara W. Leung, Milo B. Fasken, Kenneth H. Moberg[4] and Anita H. Corbett[1,6]

[1]Department of Biology, RRC 1021
Emory University
1510 Clifton Road, NE
Atlanta, Georgia 30322

[2]Emory University, Institutional Research and Academic Career Development Award (IRACDA), Fellowships in Research and Science Teaching (FIRST) Postdoctoral Fellowship

[3]Genetics and Molecular Biology Graduate Program
Emory University
1510 Clifton Rd., NE
Atlanta, GA 30322

[4]Department of Cell Biology
Emory University School of Medicine
615 Michael Street
Atlanta, Georgia 30322

[5]Biochemistry, Cell and Developmental Biology Graduate Program
Emory University
1510 Clifton Rd., NE
Atlanta, GA 30322

[6]Co-corresponding Authors Phone: 404-727-4504 (DJM) and 404-421-9061 (AHC)

Running title: Analysis of RNA exosome disease-linked substitutions in *Drosophila* EXOSC3 ortholog

Keywords: Pontocerebellar Hypoplasia Type 1b (PCH1b), RNA exosome, EXOSC3, Rrp40, RNA processing/degradation

Mailing Address Co-corresponding Authors:

Derrick J. Morton
djmorto@emory.edu
Department of Biology, RRC 1081
Emory University
1510 Clifton Road., NE
Atlanta, GA 30322

Anita H. Corbett
acorbe2@emory.edu
Department of Biology, RRC 1021
Emory University
1510 Clifton Road., NE
Atlanta, GA 30322

Abstract

The RNA exosome is an evolutionary-conserved 3'-5' riboexonuclease complex critically important for both precise processing and complete degradation of a variety of cellular RNAs. The recent discovery that mutations in genes encoding structural RNA exosome subunits cause tissue-specific diseases makes defining the role of this complex within specific tissues critically important to understand the basis of these diseases. Mutations in the RNA exosome component 3 (*EXOSC3*) gene cause Pontocerebellar Hypoplasia Type 1b (PCH1b), an autosomal recessive neurologic disorder. The disease-causing mutations are missense mutations that alter evolutionarily-conserved regions of EXOSC3. The tissue-specific defects caused by these amino acid changes in EXOSC3 are challenging to understand based on current models of RNA exosome function with only limited analysis of the complex in any multicellular model *in vivo*. The goal of this study is to provide insight into how mutations in *EXOSC3* impact the function of the RNA exosome. To assess the tissue-specific roles and requirements for the *Drosophila* ortholog of EXOSC3 termed Rrp40, we utilized tissue-specific RNAi drivers. Depletion of Rrp40 in different tissues reveals a general role for Rrp40 in the development of many tissues, but also highlight an age-dependent requirement for Rrp40 in neurons. To assess the functional consequences of the specific amino acid substitutions in EXOSC3 that cause PCH1b, we used CRISPR/Cas9 gene editing technology to generate flies that model this RNA exosome-linked disease. While these files show reduced viability, the surviving animals exhibit a spectrum of behavioral and morphological phenotypes. Furthermore, RNA-seq analysis of the *Drosophila Rrp40* mutants reveal increases in the steady-state levels of specific mRNAs and ncRNAs, some of which are central to neuronal function. In particular, *Arc1* mRNA, which encodes a key regulator of synaptic plasticity, is increased in the *Drosophila Rrp40* mutants. Taken together, this study defines a requirement for the RNA exosome in specific tissues/cell types and provides insight into how defects in RNA exosome function caused by specific amino acid substitutions that occur in PCH1b can contribute to neuronal dysfunction.

Author Summary

Pontocerebellar Hypoplasia Type 1b (PCH1b) is a devastating genetic neurological disorder that preferentially affects specific regions of the brain. Typically, children born with PCH1b have structural defects in regions of the brain associated with breathing and do not survive beyond infancy. Currently, there is no cure or treatment for the disease. PCH1b is caused by mutations in the RNA exosome component 3 (*EXOSC3*) gene, which encodes a structural component of the ubiquitous and essential multi-subunit RNA exosome complex. The RNA exosome is critical for both precise processing and turnover of multiple classes of RNAs. To elucidate the functional consequences of amino acid changes in EXOSC3 that cause PCH1b, we exploited well-established genetic approaches in *Drosophila melanogaster* to model *EXOSC3* mutations found in individuals with PCH1b. Using this system, we find that the *Drosophila* EXOSC3 homolog (termed Rrp40) is essential for normal development and has an age-dependent important function in neurons. Furthermore, PCH1b missense mutations in *Rrp40* cause reduced viability and produce neuronal-specific phenotypes that can be correlated with altered levels of target RNAs that encode factors with key roles in neurons. These results provide a basis for understanding how amino acid changes that occur in the RNA exosome contribute to neuronal dysfunction and disease.

Introduction

Precise production of both coding and non-coding RNAs requires regulation not only at the level of transcription, but also post-transcriptional events that ensure precise processing and regulated turnover [1-3]. The significance of post-transcriptional control of gene expression is underscored by the number of diseases associated with defects in RNA processing, surveillance and/or decay machinery. Specifically, mutations in genes encoding structural subunits of the ubiquitously expressed RNA exosome, a critical mediator of both RNA processing and decay, cause a variety of tissue-specific diseases [3-5].

The evolutionarily conserved RNA exosome complex, first identified in *Saccharomyces cerevisiae* [1, 2, 6], plays critical roles in RNA processing, decay and surveillance. The multi-subunit structure of the RNA exosome complex, which is conserved from archaea to humans, consists of ten subunits [1, 2, 7, 8]. In humans, the RNA exosome subunits are termed EXOSome Component (EXOSC) proteins. In *S. cerevisiae* and *Drosophila*, most RNA exosome subunits are termed Rrp proteins after the original yeast genetic screen for ribosomal RNA processing (*rrp*) mutants [6]. As illustrated in the **Fig 1A**, the complex is comprised of a catalytically inert core consisting of a hexameric 'ring' of RNase Pleckstrin homology (PH)-like domain-containing core subunits 'capped' by a trimer of S1/KH putative RNA binding domain-containing cap subunits and a catalytically active 3' to 5' processive exo- and endoribonuclease, DIS3, which associates with the bottom of the 'ring-like' core. In *S. cerevisiae*, all core RNA exosome genes are essential [1, 2, 9]. Furthermore, in *Drosophila* all RNA exosome genes studied thus far (*Dis3, Mtr3, Rrp6, Rrp41, Rrp42)* are essential and required for normal fly development [10, 11]. Studies in mice have been limited to assessing the role of *Exosc3* in B-cells *ex vivo* [12].

Given that the RNA exosome is essential for viability in model organisms examined thus far, it is surprising that mutations in genes encoding RNA exosome subunits were identified as the cause of several tissue-specific genetic diseases. Mutations in genes that encode structural subunits of the RNA exosome have now been linked to genetic diseases with distinct clinical presentations [reviewed in [13, 14]]. The first such example was the finding that recessive mutations in the *EXOSC3* gene, encoding a structural RNA exosome cap subunit (**Fig 1A**), cause a neurologic disease termed Pontocerebellar Hypoplasia type 1b (PCH1b) [3, 15]. PCH1b is characterized by hypoplasia/atrophy of the cerebellum and pons that leads to severe motor and cognitive impairments with Purkinje cell abnormalities and degeneration of spinal motor neurons [15-17]. A

number of missense mutations that cause single amino acid substitutions in conserved regions of EXOSC3 have been linked to PCH1b. Of note, clinical reports indicate that the severity of PCH1b pathology is influenced by *EXOSC3* allelic heterogeneity, suggesting a genotype-phenotype correlation [5, 18, 19]. These findings indicate that EXOSC3 plays a critical role in the brain and suggest specific functional consequences for amino acid changes linked to disease.

A previous study that modeled loss of *EXOSC3* in zebrafish by knockdown with antisense morpholinos reported embryonic maldevelopment, resulting in small brain size and reduced motility [5]. While co-injection of wild-type zebrafish *exosc3* mRNA could rescue these phenotypes, mutant *exosc3* containing mutations modeling PCH1b failed to rescue [5], suggesting that these mutations disrupt the normal function of EXOSC3. Other studies to assess the functional consequences of RNA exosome disease-linked amino acid changes in RNA exosome subunits have only been performed thus far in yeast [20, 21] providing little insight into how these specific changes could cause tissue-specific consequences. Thus, no studies have produced a genetic model to explore the functional consequences of amino acid changes that cause disease in a multi-cellular model *in vivo*.

In this study, we exploit *Drosophila* as a model to understand the tissue-specific roles and requirements for Rrp40, the *Drosophila* ortholog of EXOSC3. This system also provides an *in vivo* platform to test the functional consequences of amino acid substitutions linked to disease by employing CRISPR/Cas9 gene editing technology to create an allelic series of mutations to model the amino acid substitutions that occur in PCH1b. This work reveals a critical role for Rrp40 in neurons during development and demonstrates that mutations in *Rrp40* in flies that model genotypes in individuals with PCH1b cause reduced viability and neuronal-specific behavioral phenotypes. Mutant flies display a broad range of phenotypes, providing insight into how distinct amino acid changes alter RNA exosome function. Moreover, RNA-sequencing analysis reveals that *Rrp40* mutants modeling different patient genotypes show specific differences in mRNAs and ncRNAs in each mutant providing a molecular basis for the phenotypes observed. We identify the neuronal gene *Arc1*, a critical regulator of neuronal function, increased in the RNA-seq dataset for both *Rrp40* mutants, underscoring the critical role of the RNA exosome regulating key transcripts in neurons. Taken together, our results provide the first evidence for a critical function of the RNA exosome subunit Rrp40 in neurons. We show that the *Drosophila* model can be used to

provide insight into tissue-specific function of the RNA exosome *in vivo* to explore the functional consequences of amino acid substitutions linked to distinct disease phenotypes.

Results

The RNA exosome subunit Rrp40 is essential for development.

To examine *in vivo* requirements for Rrp40 we employed RNAi to deplete Rrp40 from specific tissues/cell types. A small panel of four *Gal4* lines with distinct expression patterns, *Actin5c>Gal4* (global), *elav>Gal4* (neurons), *repo>Gal4* (glia) and *Mhc>Gal4* (muscle), was used in combination with an RNAi transgene targeting the *Drosophila* EXOSC3 homolog Rrp40 (TRiP *HMJ23923*). Expression of each *Gal4* driver to deplete *Rrp40* led to complete lethality, with no surviving adults (**Fig 1B**). This general developmental requirement for *Rrp40* in multiple tissues is consistent with previous studies of other RNA exosome subunits in *Drosophila* [10, 11].

To bypass the embryonic requirement for *Rrp40,* we employed a temperature shift strategy to control the stage of RNAi depletion. As depicted in **Fig 1C**, a ubiquitously expressed, temperature-sensitive *tubulin(tub)-Gal80^{ts}* transgene was used to deplete *Rrp40* in combination with the panel of *Gal4* drivers. RNAi was induced by a shift from the permissive to restrictive temperature (18°C to 29°C) 24 hours after egg laying. Global *Rrp40* depletion (*Actin5c>Gal4*) using this temperature-shift still produced no adults, indicating complete lethality; however, *Rrp40* depletion at this time-point in neurons and glia allowed a low level of adult viability (**Fig 1D**). Depletion of *Rrp40* in wild-type flies in muscle produced a mild survival defect. Intriguingly, adult survivors of neuronal *Rrp40* depletion had severely reduced lifespans (~1-2 days) relative to both *Gal4* driver alone and wild-type controls. By contrast, the lifespan of survivors of the glial or muscle depletion was indistinguishable from both controls (**Fig 1E**). In sum, these RNAi data argue for a strict requirement for *Rrp40* and thus RNA exosome function in multiple tissues during embryonic development. Bypassing this embryonic requirement reveals an enhanced requirement for Rrp40 in neurons compared to other tissues during later stages of development and adult homeostasis.

PCH1b mutations engineered into the *Rrp40* locus impair viability and shorten lifespan.

As shown in **Fig 2A**, The EXOSC3/Rrp40 protein consists of three domains: an N-terminal domain, an S1 putative RNA binding domain, and a K-homology (KH) putative RNA binding domain. Notably, the human

EXOSC3 Glycine 31 [G31] residue and the analogous *Drosophila* G11 residue are located in a conserved region within the N-terminal domain while EXOSC3 Aspartate 132 [D132] and the analogous *Drosophila* D87 residue are both located in a conserved region within the S1 domain **(Fig 2A)**. Thus, EXOSC3 amino acid substitutions that cause disease occur in regions that are evolutionarily conserved across species.

We utilized CRISPR/Cas9-mediated genome editing technology to create alleles corresponding to amino acid substitutions in Rrp40 that cause PCH1b disease (**Fig 2B**). As illustrated in **Fig 2B**, *Drosophila* allows for true modeling of both homozygous and heterozygous alleles that cause disease. In parallel, a control *Rrp40* chromosome was also created using a wildtype Homology Directed Repair (HDR) donor template to create flies we refer to as *Rrp40*^{wt} that had undergone the same editing process as flies with engineered amino acid substitutions. As described in Materials and methods, all three *Rrp40* alleles created (*Rrp40*^{wt}*, Rrp40*^{G11A}*, and Rrp40*^{D87A}) contain the *3xP3-DsRed* cassette, which allows for visual sorting by red fluorescence in eye tissue, inserted in the intergenic region downstream of the *Rrp40 3'UTR* (**S1 Fig**). As described in Materials and methods, HDR donor templates containing *3xP3-DsRed* were injected into *nos*-Cas9-engineered embryos. To confirm that the precisely targeted events had occurred in DsRed-positive flies, we extracted genomic DNA, amplified and sequenced the engineered region in both the Rrp40 wild-type (*Rrp40*^{wt}) control and flies containing missense mutations (independent flies, n=5) (*Rrp40*^{G11A} and *Rrp40*^{D87A}) (**S2 Fig**).

Initial analysis of these missense *Rrp40* alleles revealed reduced homozygote viability to adulthood within intercrosses of heterozygous parents (*Rrp40*^{G11A}: 14% of expected, n=126, and *Rrp40*^{D87A}: 38% of expected, n=182) (**Fig 2B**). In contrast, *Rrp40*^{wt} control flies eclose at a rate comparable to *w*^{1118}. The numbers of surviving adults were further reduced by placing *Rrp40*^{G11A} or *Rrp40*^{D87A} over a genomic deletion (*Df(2L) Exel600*) that removes the *Rrp40* locus, suggesting that both of these missense alleles are hypomorphs, rather than amorphs or hypermorphs (**Fig 2B**, **S3 Fig**). The lower viability of the *Rrp40*^{G11A} allele, either *in trans* to itself or to (*Df(2L) Exel6005)*, indicates that this is a stronger loss-of-function allele than *Rrp40*^{D87A}.

Significantly, flies with the engineered *Rrp40*^{wt} allele have a similar lifespan to control *wild-type* (*w*^{1118}) flies within the tested 30-day testing period, showing that the *3xP3-DsRed* cassette inserted into the intergenic region downstream of *Rrp40* does not appreciably impair survival (**Fig 2C**), thus *Rrp40*^{wt} was included as a control for subsequent studies. In contrast to Rrp40^{wt}, Kaplan-Meier plots of *Rrp40*^{G11A} homozygotes and *Rrp40*^{D87A} homozygotes reveal significantly impaired survival, with all *Rrp40*^{D87A} animals dead by day 25 and all

Rrp40^{G11A} homozygotes dead by day 14 (**Fig 2C**). Among PCH1b individuals, *EXOSC3* (p. Asp132Ala) missense alleles can occur as homozygotes, but produce more severe disease *in trans* to nulls alleles [5, 17, 19]. Consistent with this pattern, the (*Df(2L) Exel6005)* deletion removing *Rrp40* significantly decrease the survival of *Rrp40*^{D87A} flies exacerbates *Rrp40*^{D87A} survival (**Fig 2C**).

Rrp40 mutant flies exhibit age-dependent morphological and behavioral defects.

Rrp40^{G11A} and *Rrp40*^{D87A} adult survivors exhibit wing posture and behavior defects that are consistent with neurological deficits. *Rrp40*^{G11A} and *Rrp40*^{D87A} adults position their wings in an abnormal “held-up and -out” posture rather than folding them together over the dorsal surface of the thorax and abdomen (**Fig 3A**) and this phenotype worsens with age (**Fig 3B**). *Rrp40*^{G11A} and *Rrp40*^{D87A} mutant animals also show reduced locomotor activity in a negative geotaxis assay that become more severe with age (**Fig 3C**). Both genotypes also display seizure-like behaviors and extended periods of inactivity (**S1 Video**) relative to age-matched control *Rrp40*^{wt} flies. The severity of the wing posture and locomotor defects among *Rrp40* alleles followed a similar pattern: *Rrp40*^{G11A} causes a more severe phenotype than *Rrp40*^{D87A}, which is in turn is enhanced by (*Df(2L) Exel6005)*. Notably, this pattern of phenotypes mimics the pattern of disease severity observed among individuals with PCH1b.

Pan-neuronal expression of human _EXOSC3_ is sufficient to rescue behavioral phenotypes in _Rrp40_ mutant flies.

To ensure that phenotypes observed are due to altered Rrp40 function and explore functional conservation between Rrp40 and human EXOSC3, we created transgenic flies that express human *EXOSC3-myc* from an inducible driver. The *UAS-EXOSC3-myc* transgene was expressed only in the neurons (*elav>Gal4*) of *Rrp40* mutant animals (**Fig 4A**). Notably, *UAS-EXOSC3-myc* produced a mild but consistent rescue of *Rrp40* mutant locomotor defects in the absence of the *Gal4* driver (*rescue control*, **Fig 4B**), suggesting leaky expression from the transgene. Addition of the *elav>Gal4* driver led to a robust rescue of climbing behavior: *Rrp40* mutant animals with neuronal expression of *EXOSC3* (*elav>EXOSC3*) perform normally in locomotor assays (**Fig 4B**), indicating that human EXOSC3 can restore functions that are lacking in *Rrp40* mutant neurons.

Steady-state levels of RNA exosome subunit levels are not grossly affected in *Rrp40* mutant flies.

Amino acid substitutions in Rrp40 could alter protein steady-state levels or impact the levels of the RNA exosome complex components. To test this possibility *in vivo*, we compared wild-type and Rrp40 variant steady-state levels in whole flies and head tissue. Immunoblots of RNA exosome cap subunits (Csl4, Rrp4 and Rrp40) and a core ring subunit (Mtr3) (**see Fig 1A**) show that steady-state levels of these proteins do not differ markedly in *Rrp40* mutant whole flies (**Fig 5A**) or heads (**Fig 5B**) compared to control. These data confirm that Rrp40-G11A and Rrp40-D87A proteins are present at levels comparable to wildtype Rrp40 *in vivo* and suggest that these amino acid changes in Rrp40 do not grossly destabilize the RNA exosome complex. Rather, $Rrp40^{G11A}$ and $Rrp40^{D87A}$ may affect the ability of the RNA exosome complex to target and/or degrade key RNA targets *in vivo*.

RNA-sequencing analysis of *Rrp40* alleles reveals distinct gene expression profiles.

To complement our functional studies, we performed RNA-Seq analysis on three biological replicates of adult heads for each genotype ($Rrp40^{wt}$, $Rrp40^{G11A}$ and $Rrp40^{D87A}$). Unbiased principal component analysis (PCA) of the resulting RNA expression data produced three distinct clusters (**Fig 6A**), indicating that each PCH1b-linked *Rrp40* allele alters the steady-state transcriptome relative to control $Rrp40^{wt}$, and that these two missense mutants also produce distinct effects on head RNAs relative to each other.

The high degree of reproducibility amongst the RNA-Seq replicates allowed us to identify genes mis-expressed in each of the *Rrp40* mutant backgrounds relative to wild type controls, and between the two mutant *Rrp40* alleles (**Fig 6B-C** and **S2** and **S3 Tables**). Of the total number of altered transcripts, a majority are mRNAs (61% in $Rrp40^{G11A}$ and 66% in $Rrp40^{D87A}$) and the remainder include several classes of ncRNAs (**Fig 6E**). The different classes of affected ncRNAs include lncRNA, snoRNA, asRNA, tRNA, scaRNA and sisRNA (**Fig 6F**). Consistent with the role of the RNA exosome in RNA decay, the majority of gene expression changes detected for $Rrp40^{G11A}$ or $Rrp40^{D87A}$ compared to $Rrp40^{wt}$ consist of increases in steady-state RNA transcript levels. Of 394 transcripts that change 5-fold or more in the $Rrp40^{G11A}$ mutant sample, 343 (87%) are increased (FDR<0.05), while 375 of a total of 446 transcripts that change 5-fold or more (84%) in the $Rrp40^{D87A}$ sample are increased.

To distinguish the RNA landscape of both *Rrp40* mutants, we compared both the *Rrp40*^{G11A} and *Rrp40*^{D87A} datasets to each other; there are 181 transcripts increased (Up) in *Rrp40*^{G11A} and 143 transcripts increased (Up) in *Rrp40*^{D87A} (q<0.05, >1-fold change) **(S4A Fig** and **S4 Table)**. Of transcripts that showed a statistically significant change in both mutants, 97% (n=313) are mRNAs and 3% (n=11) are ncRNAs, suggesting a predominant effect on protein coding genes **(S4B Fig)**.

Given that the primary role of the RNA exosome is RNA decay [22], we next assessed whether the *Rrp40*^{G11A} and *Rrp40*^{D87A} alleles elevate an overlapping or distinct set of RNAs (FDR<0.05, >5-fold change). This analysis found many coordinately elevated coding (181) and non-coding (110) transcripts between the two groups, but also a considerable number of RNAs that were only elevated in one mutant background (*Rrp40*^{G11A}: 65 unique coding and 20 unique non-coding; *Rrp40*^{D87A}: 124 unique coding and 30 unique non-coding) (**Fig 6D**). Thus, gene expression patterns among the *Rrp40* mutants show specific differences in both coding and non-coding transcripts in each *Rrp40* mutant, providing further evidence that the PCH1b-linked G11A and D87A substitutions in Rrp40 have distinct effects on the head/brain transcriptome. Gene Ontology (GO) analysis (FlyEnrichr; amp.pharm.mssm.edu/FlyEnrichr/) of coding transcripts significantly affected in *Rrp40*^{G11A} and *Rrp40*^{D87A} heads identified ten enriched pathways identified, including *damaged DNA binding* and *telomeric DNA binding* in the *Rrp40*^{G11A} mutant (**Fig 6G**) and *damaged DNA binding* and *RNA binding* in the *Rrp40*^{D87A} mutant (**Fig 6G**). Thus, although there is a subset of common transcripts effected in the mutants, there are also substantial differences, which could explain the genotype-phenotype correlation displayed in *Rrp40* mutant flies.

RNA-sequencing analysis reveals increased steady-state levels of key neuronal genes in *Rrp40* mutant flies.

RNA-sequencing analysis revealed increased steady-state levels of multiple functionally important neuronal genes including *Arc1* [*Rrp40*^{G11A} (30.2-fold increase); *Rrp40*^{D87A} (16.1-fold increase)], *Or82a* [*Rrp40*^{G11A} (35.1-fold increase); *Rrp40*^{D87A} (2.1-fold increase)], *PNUTS* [*Rrp40*^{G11A} (3.4-fold increase); *Rrp40*^{D87A} (3.2-fold increase)], *WFS1* [*Rrp40*^{G11A} (6.9-fold increase); *Rrp40*^{D87A} (5.6-fold increase)], and *knon* [*Rrp40*^{G11A} (23.6-fold increase); *Rrp40*^{D87A} (16.5-fold increase)] in *Rrp40* mutants (**Fig 7**). We visualized differentially expressed genes in the RNA-seq dataset, utilizing Integrative Genomics Viewer (IGV) technology for *Arc1* (**Fig 7A**), *Or82a, PNUTS, WFS1* and *knon (CG7813)* reads (**S5 Fig**). To validate altered gene expression from RNA-seq analysis,

RT-qPCR was performed as shown in **Fig 7B** and **C**. RT-qPCR confirmed that steady-state levels of *Arc1* mRNA in *Rrp40* mutants (*Rrp40*^{G11A} and *Rrp40*^{D87A}) are significantly increased as compared to control (*Rrp40*^{wt}) (**Fig 7B**). As an additional measure of validation by RT-qPCR, we analyzed *CG8617* (**Fig 7B**), a neighboring gene of *Arc1* that showed no change in RNA-seq reads (**Fig 7A**). To extend the validation, we analyzed target transcripts increased in both *Rrp40* mutants compared to *Rrp40*^{wt}, including *Or82a, PNUTS, WFS1* and *knon* (**Fig 7C**). Next, we tested whether expression of wild-type human *EXOSC3 (UAS-EXOSC3-myc)* only in neurons could rescue increased steady-state levels of validated transcripts, including *Arc1* and *WFS1*. RT-qPCR confirmed that steady-state levels of these transcripts are significantly decreased compared to control UAS alone (-), when *EXOSC3* is expressed in neurons using a *Gal4* driver (+*Gal4*) (**Fig 7D)**. These results validate our RNA-seq analysis as well as highlight transcripts that may be potential regulators of neuronal function, providing candidates to help define the molecular mechanism for the phenotypes observed in both *Rrp40* mutants.

Discussion

In this study, we generated a *Drosophila* model to explore the requirement for RNA exosome function in specific tissues/cell types and define the functional consequences of amino acid substitutions in structural subunits of this complex that are linked to human disease. We provide evidence that the *Drosophila* Rrp40 subunit is essential for normal fly development and viability, consistent with earlier studies of other RNA exosome subunits in *Drosophila* [10-12, 18]. This analysis reveals an age-dependent requirement for Rrp40 in neurons critical for later stages of development and adult homeostasis. We provide evidence that missense mutations in *Rrp40* in flies, which model genotypes in individuals with PCH1b, cause reduced viability and produce neuronal-specific behavioral phenotypes that align with PCH1b severity, revealing a genotype-phenotype correlation. Moreover, RNA-sequencing of the brain-enriched transcriptome of *Rrp40* mutant flies identifies specific changes in both coding RNAs, including the synaptic regulator *Arc1*, and non-coding RNAs, consistent with impaired RNA exosome activity. These data establish a critical role for the RNA exosome in neurons and provide an initial characterization of the functional consequences of amino acid changes that underlie PCH1b *in vivo* using a multicellular organism.

Previous studies of the RNA exosome have provided evidence that individual subunits of this complex are essential in the organisms analyzed [1, 2, 9-12]. Thus, identification of mutations in genes encoding structural

subunits of the RNA exosome that cause tissue-specific pathology was unexpected. In fact, only a few studies have explored the requirement for the RNA exosome in any specific tissues or cell types [11, 23-25]. Prior work using methods to deplete individual subunits of the complex in *Drosophila*, revealed that these subunits are essential [11, 26]. More recent work examining the role of the EXOSC3 subunit in human embryonic stem cells built on studies that have implicated the RNA exosome in restraining differentiation [23-25]. If there are specific requirements for the RNA exosome that are most critical for the development and/or homeostasis of certain cells or tissues, this could explain why mutations that impair the function of this complex could preferentially affect certain tissues. Indeed, our studies exploiting *Drosophila* uncover an age-dependent requirement for Rrp40 in neurons. However, mutations in multiple genes that encode structural subunits of the RNA exosome termed exosomopathies, including two cap subunit genes *EXOSC3* [5, 18, 27-29] and *EXOSC2* [4] and two core subunit genes *EXOSC8* [3] and *EXOSC9* [30, 31], have now been linked to genetic diseases with a variety of clinical presentations reported. The finding that multiple mutations that likely impair the function of the RNA exosome cause different clinical consequences is not consistent with a model where a defined tissue or cell type is highly dependent on the function of this complex. Rather the missense mutations that have been identified in multiple RNA exosome subunit genes likely impair tissue-specific functions of this complex. Indeed, although the number of patients for any given exosomopathy is small, there are now multiple missense mutations that have been identified, raising the questions of whether different amino acid changes that occur within the same RNA exosome gene impair the function of the complex in the same manner or to the same extent. A combination of approaches can be employed to understand how the amino acid changes that occur in patients affect the function of the RNA exosome.

A possibility with any missense mutation is that the amino acid substitution introduced leads to the destabilization of the protein encoded. In fact, a previous study using patient fibroblast or myoblasts to examine variants of EXOSC8, a RNase (PH)-like domain-containing core 'ring' subunit linked to another form of PCH [30, 31], not only showed reduced levels of the EXOSC8 variants, but also EXOSC3, indicating that defects in core 'ring' subunits of the RNA exosome can lead to a reduction in other subunits [3]. This finding is rather surprising given that the patients analyzed did not exhibit pathology related to the cell types analyzed. Our analysis shows that the steady-state levels of Rrp40 protein and other RNA exosome cap or ring subunits do not differ markedly in *Rrp40*^{G11A} and *Rrp40*^{D87A} mutant flies as compared to control (e.g. see **Fig 5A** and **B**) in either whole flies or

isolated heads. These findings suggest that overall loss of the RNA exosome complex is not the primary defect that occurs at least in the *Drosophila* model.

To consider how amino acid substitutions in EXOSC3 could impact the overall RNA exosome complex, we can take advantage of the availability of structures of this large macromolecular complex [7, 8, 32-34]. While there is no structure available of the *Drosophila* RNA exosome, the considerable evolutionary conservation illustrated in **Fig 2B** provides some context to consider how distinct amino acid changes in EXOSC3/Rrp40 could impair RNA exosome function. As shown in **Fig 2A**, the amino acid changes modeled in this study lie within the N-terminal (G31A) and S1 (D132A) domains of EXOSC3/Rrp40. The G31 residue in EXOSC3 packs against the surface of EXOSC5 and, therefore, the EXOSC3-G31A substitution could impair the interaction of EXOSC3 with EXOSC5 [7]. The D132 residue in EXOSC3 is located in a loop between strands in the S1 domain and the D132A substitution could thus impair the folding of the loop and, subsequently, disturb interactions between EXOSC5 and EXOSC9 [7]. These observations suggest that PCH1b amino acid changes in EXOSC3 could impair interactions with other RNA exosome subunits, leading to compromised RNA exosome complex integrity; however, wholesale loss of the RNA exosome seems unlikely to explain the phenotypic variability reported in PCH1 [35].

Ultimately, any change in the function of the RNA exosome should affect processing or degradation of target RNAs and those changes should dictate phenotype. Beyond a change in the overall levels of the RNA exosome complex, there are at least two additional mechanisms that could interfere with the function of the complex. First, amino acid substitutions could directly alter interactions with specific target RNAs. In budding yeast, the three cap subunits of the RNA exosome make direct contact with RNA [8, 33], and the integrity of the S1/KH cap subunit ring is critical for the path of RNA to Rrp6, the nuclear catalytic subunit of the exosome [33]. Second, defects in RNA exosome subunits could differentially affect interaction with different RNA exosome cofactors. A variety of cofactors associate with the RNA exosome to confer specificity for target RNAs and/or facilitate the unwinding of structured RNAs [34]. Indeed, structural studies show that the nuclear RNA exosome cofactor Mpp6 interacts with the Rrp40 cap subunit [33, 36], and that an amino acid change in Rrp40 that models a change in PCH1b decreases the interaction of Mpp6 with the RNA exosome [36]. The idea that interactions with specific cofactors could be perturbed by the amino acid changes that occur in disease is attractive because altered interactions with cofactors in different tissues or cell types could explain the phenotypic variation

observed for mutations within the same *EXOSC* gene or the different *EXOSC* subunit genes that are linked to distinct diseases. To explore the idea that altered cofactor interactions contribute to pathology, studies to identify RNA exosome cofactors from different tissues would need to be undertaken.

To begin to explore the specific RNA targets affected by missense mutations in *EXOSC3/Rrp40*, we performed RNA-Seq analysis. Our brain-enriched RNA-sequencing data on *Rrp40* mutant flies show a global increase in transcripts and specific differences in both coding and non-coding transcripts in each *Rrp40* mutant compared to control (**Fig 6B** and **C**). The finding that more RNAs show an increase in steady-state levels as compared to a decrease is consistent with impairing the function of a complex required for RNA turnover. Intriguingly, levels of a critical synaptic regulator, *Arc1,* are markedly increased in both *Rrp40* mutants, suggesting that the RNA exosome regulates key neuronal transcripts. Critically, these data provide insight into how amino acid changes in Rrp40 could alter RNA exosome function by disruption of processing and/or decay of transcripts required for proper development/maintenance of the nervous system.

In this study, we modeled three patient genotypes associated with PCH1b (**Fig 2B**). The analysis reveals a range of phenotypes, suggesting a genotype-phenotype correlation. Furthermore, the spectrum of phenotypes observed in flies expressing alleles of PCH1b aligns with some aspects of genotype-phenotype correlations reported for individuals with PCH1b [29, 35], suggesting that these amino acid changes differentially impact RNA exosome activity. For example, homozygous PCH1b *EXOSC3* (p. Gly31Ala) mutations [5, 17, 29], modeled as *Drosophila Rrp40*^{G11A}, cause severe phenotypes (**Fig 3**). In contrast, homozygous PCH1b *EXOSC3* (p. Asp132Ala) mutations, modeled as *Drosophila Rrp40*^{D87A}, cause moderate phenotypes as compared to the *Rrp40*^{G11A} mutant flies. Moreover, PCH1b *EXOSC3* (p. Asp132Ala) *in trans* to a probable *EXOCS3* null mutation, modeled as *Drosophila Rrp40*$^{D87A/Df(2L)}$ causes the most severe phenotypes [5], arguing that *D132A* is likely hypomorphic. Interestingly, *EXOSC3* (p. Gly31Ala) *in trans* to a probable *EXOCS3* null has not been reported in individuals with PCH1b, and the lethality of the corresponding genotype *Rrp40*$^{G11A/Df(2L)}$ in flies (**S3 Fig)**, suggests that G31A and G11A are strong loss of function alleles. Remarkably, alleles of PCH1b expressed in *Drosophila* reveal phenotypes that align with reported severity in individuals with PCH1b, albeit the clinical phenotypes are highly variable [29, 35]; however, it is important to note that pathology and/or disease severity could arise from a combination of effects, and these combined effects could be specific to the genetic background of the patients.

Critically, the number of reported individuals with EXOSC3-related PCH1b is small [5, 17, 27-29, 37], thus limiting the ability to make genotype-phenotype correlations in patients and highlighting the value of the fly model.

In summary, this study identifies a critical role for Rrp40 in both development and viability in *Drosophila* along with an age-dependent requirement for Rrp40 in neurons. Using CRISPR/Cas9 gene editing technology and *Drosophila* genetic approaches, we modeled PCH1b-linked EXOSC3 amino acid changes in Rrp40, which reveal neuronal-specific phenotypes and define RNA targets critical for neuronal function. Strikingly, both behavioral phenotypes of *Rrp40* mutant flies and levels of RNA targets are rescued by pan-neuronal transgenic expression of human *EXOSC3*. Taken together, these results demonstrate that this model can be utilized to explore the broader consequences of amino acid changes in the RNA exosome.

Materials and methods

Drosophila Stocks

Crosses were maintained in standard conditions at 25°C unless otherwise noted. Stocks used in this study: w^{1118}, *UAS-Rrp40*^{RNAi} (TRiP *HMJ23923*, *BDSC #63834*), *Df(2L)Exel6005* (*BDSC #7492)*, *Tub>Gal80*^{ts} (*BDSC #7017*), and the following Gal4 stocks: *Actin5c>Gal4 (BDSC#25374)*, *elav>Gal4 (BDSC#458)*, *repo>Gal4 (BDSC#7415)* and *Mhc>Gal4 (BDSC#55133)* were obtained from the Bloomington *Drosophila* Stock Center. *Rrp40*^{G11A} and *Rrp40*^{D87A} were generated by CRISPR/Cas9 editing (detail below) at Bestgene, Inc. (CA).

Generation of CRISPR/Cas9 Flies

Molecular Reagents

pU6-gRNAs: Target-specific sequences were identified sequences using DRSC flyCRISPR optimal target finder (https://www.flyrnai.org/crispr/) for Rrp40 and gRNAs were synthesized as 5'-phosphorylated oligonucleotides, annealed, and ligated into the *Bbs*I sites of pU6-*Bbs*I chiRNA [38].

Homology-directed repair (HDR) templates: HDR donor vectors (Emory Integrated Genomic Core) were constructed by cloning a 3kb fragment of the *Rrp40* locus, including a loxP-flanked *3xP3-DsRed* cassette inserted downstream of the *Rrp40 3'UTR*, into *KpnI/SmaI* sites of the *pBlueScript-II* vector. Base changes corresponding to G11A and D87A were engineered into this backbone. The *3xP3-DsRed* cassette allows positive selection based on red-fluorescence in the adult eye [39].

CRISPR-transformants: Injection of DNA mixtures (500 ng/μl HDR and 250 ng/μl U6-gRNA plasmid) into *nos-Cas9* embryos and subsequent screening for dsRed+ transformants was performed by Bestgene, Inc. CRISPR. Edits were confirmed by direct sequencing (**S2 Fig**).

Lifespan Analysis

Lifespan was assessed at 25°C as described previously[40]. In brief, newly eclosed animals were collected, separated by sex, placed in vials (up to 20 per vial), and transferred to fresh vials weekly. Survivorship was scored daily. At least 8 vials of each genotype were tested and averaged to calculate mean and standard deviation.

Behavioral Assays

Negative-geotaxis assay was performed as previously described [41] with some modification. Newly eclosed flies (day 0) were collected, divided into groups of 10 of 10 flies, and kept in separate vials. Cohorts of age-matched flies were then transferred to a 25-ml graduated for analysis of climbing response. At least 10 groups (i.e. ~100 flies) were analyzed per genotype.

Immunoblotting

Protein lysates of whole flies or heads were resolved on 4–20% Criterion TGX polyacrylamide gels (Bio Rad), transferred to nitrocellulose membranes, incubated for ≥1hr in blocking buffer (5% non-fat dry milk in 0.1% TBS-Tween), followed by an overnight incubation at 4°C in primary antibody diluted in blocking buffer. Primary antibodies were detected using species-specific horse radish peroxidase (HRP) conjugated secondary antibodies (Jackson ImmunoResearch) and enhanced chemiluminescence (ECL, Sigma). Primary antibodies include: guinea pig anti-Rrp4 (1:1000), rabbit anti-Rrp40 (1:1000), guinea pig anti-Csl4 (1:000), and rat anti-Mtr3 (1:1000) gift of the Lis lab [26].

RNA Sequencing Analysis

RNA-seq was performed on three replicates of 60 newly-eclosed adult heads per genotype (*Rrp40*^{G11A}, *Rrp40*^{D87A} and *Rrp40*^{wt}). Heads were collected and lysed in TRIzol (ThermoFisher). rRNA was depleted and cDNA libraries were prepared using Truseq RNA sample prep kit (Illumina). The cDNA paired-end reads were sequenced at the Georgia Genomics and Bioinformatics Core at UGA using a NextSeq (150 cycles) PE75 High Output Flowcell. The reads were mapped to the BDGP *D. melanogaster* (r6.25) genome. Several sequence datasets were downloaded from GenBank and FlyBase for initial assessment of the data including: 1) All Drosophila ribosomal sequences found in Genbank: *Drosophila*_rRNA.fa**;** 2) All FlyBase *D. melanogaster* transcripts from assembly r6.25: dmel_transcripts_r6.25.fa**.** DESeq2 was used with default settings for transcript assembly. The resulting assembled transcripts were compared using DESeq2 to identify genes that change significantly (p-value<0.05, >1.5-fold change) in expression. Only genes that were significantly changed compared to the control CRISPR line, *Rrp40*^{WT}, were used for further analysis.

RNA Isolation and qPCR

Total RNA was isolated from heads with TRIzol (Invitrogen) and treated with Turbo DNase (Invitrogen) to degrade contaminating DNA. For qRT-PCR analyses, cDNA was generated using MMLV Reverse transcriptase (Invitrogen) from 1 µg of total RNA, and then used as template for quantitative real-time PCR (qPCR) from duplicate samples of 10 ng cDNA with QuantiTect SYBR Green Master Mix using an Applied Biosystems StepOne Plus real time machine (ABI). Results were analyzed using the ΔΔCT method and normalized to *Act5c* as fold change relative to control. Oligonucleotide sequences are provided in (**S1 Table)**.

Acknowledgements

This work was supported by both a National Institutes of Health F32 grant (GM125350) and a Postdoctoral Enrichment Award from the Burroughs Wellcome Fund to D.J.M, National Institutes of Health F31 grants to B.J. (NS103595) and J.C.R (HD088043), a National Institutes of Health R01 grant (MH107305) to A.H.C. and K.H.M, and a National Institutes of Health R01 grant (GM130147) to A.H.C. D.J.M. was also supported by the Emory University National Institutes of Health Institutional Research and Academic Career Development Award (IRACDA) (GM000680) Fellowships in Research and Science Teaching (FIRST) Postdoctoral Fellowship.

Author Contributions

Conceptualization: Derrick J. Morton, Sara W. Leung, Milo B. Fasken, Kenneth H. Moberg, Anita H. Corbett

Data curation: Derrick J. Morton

Formal analysis: Derrick J. Morton, Kenneth H. Moberg, Anita H. Corbett

Funding acquisition: Derrick J. Morton, Binta Jalloh, Kenneth H. Moberg, Anita H. Corbett

Investigation: Derrick J. Morton, Binta Jalloh, Lily Kim, Isaac Kremsky, Thalia Le, Khuong B. Nguyen, J. Christopher Rounds, Maria C. Sterrett, Brianna Brown

Methodology: Derrick J. Morton, Kenneth H. Moberg, Anita H. Corbett

Project administration: Derrick J. Morton, Kenneth H. Moberg, Anita H. Corbett

Supervision: Derrick J. Morton, Kenneth H. Moberg, Anita H. Corbett

Writing - original draft: Derrick J. Morton, Anita H. Corbett

Writing - review & editing: Derrick J. Morton, Kenneth H. Moberg, Anita H. Corbett

References

1. Mitchell P, Petfalski E, Shevchenko A, Mann M, Tollervey D. The exosome: a conserved eukaryotic RNA processing complex containing multiple 3'-->5' exoribonucleases. Cell. 1997;91(4):457-66. Epub 1997/12/09. doi: 10.1016/s0092-8674(00)80432-8. PubMed PMID: 9390555.
2. Allmang C, Petfalski E, Podtelejnikov A, Mann M, Tollervey D, Mitchell P. The yeast exosome and human PM-Scl are related complexes of 3' --> 5' exonucleases. Genes Dev. 1999;13(16):2148-58. Epub 1999/08/31. doi: 10.1101/gad.13.16.2148. PubMed PMID: 10465791; PubMed Central PMCID: PMCPMC316947.
3. Boczonadi V, Muller JS, Pyle A, Munkley J, Dor T, Quartararo J, et al. EXOSC8 mutations alter mRNA metabolism and cause hypomyelination with spinal muscular atrophy and cerebellar hypoplasia. Nat Commun. 2014;5:4287. Epub 2014/07/06. doi: 10.1038/ncomms5287. PubMed PMID: 24989451; PubMed Central PMCID: PMCPMC4102769.
4. Di Donato N, Neuhann T, Kahlert AK, Klink B, Hackmann K, Neuhann I, et al. Mutations in EXOSC2 are associated with a novel syndrome characterised by retinitis pigmentosa, progressive hearing loss, premature ageing, short stature, mild intellectual disability and distinctive gestalt. J Med Genet. 2016;53(6):419-25. Epub 2016/02/05. doi: 10.1136/jmedgenet-2015-103511. PubMed PMID: 26843489.
5. Wan J, Yourshaw M, Mamsa H, Rudnik-Schoneborn S, Menezes MP, Hong JE, et al. Mutations in the RNA exosome component gene EXOSC3 cause pontocerebellar hypoplasia and spinal motor neuron degeneration. Nat Genet. 2012;44(6):704-8. Epub 2012/05/01. doi: 10.1038/ng.2254. PubMed PMID: 22544365; PubMed Central PMCID: PMCPMC3366034.
6. Mitchell P, Petfalski E, Tollervey D. The 3' end of yeast 5.8S rRNA is generated by an exonuclease processing mechanism. Genes Dev. 1996;10(4):502-13. Epub 1996/02/15. doi: 10.1101/gad.10.4.502. PubMed PMID: 8600032.
7. Liu Q, Greimann JC, Lima CD. Reconstitution, activities, and structure of the eukaryotic RNA exosome. Cell. 2006;127(6):1223-37. Epub 2006/12/19. doi: 10.1016/j.cell.2006.10.037. PubMed PMID: 17174896.
8. Makino DL, Conti E. Structure determination of an 11-subunit exosome in complex with RNA by molecular replacement. Acta Crystallogr D Biol Crystallogr. 2013;69(Pt 11):2226-35. Epub 2013/11/06. doi: 10.1107/S0907444913011438. PubMed PMID: 24189234; PubMed Central PMCID: PMCPMC3817696.
9. Briggs MW, Burkard KT, Butler JS. Rrp6p, the yeast homologue of the human PM-Scl 100-kDa autoantigen, is essential for efficient 5.8 S rRNA 3' end formation. J Biol Chem. 1998;273(21):13255-63. Epub 1998/05/28. doi: 10.1074/jbc.273.21.13255. PubMed PMID: 9582370.
10. Hou D, Ruiz M, Andrulis ED. The ribonuclease Dis3 is an essential regulator of the developmental transcriptome. BMC Genomics. 2012;13:359. Epub 2012/08/03. doi: 10.1186/1471-2164-13-359. PubMed PMID: 22853036; PubMed Central PMCID: PMCPMC3434026.
11. Lim SJ, Boyle PJ, Chinen M, Dale RK, Lei EP. Genome-wide localization of exosome components to active promoters and chromatin insulators in Drosophila. Nucleic Acids Res. 2013;41(5):2963-80. Epub 2013/01/30. doi: 10.1093/nar/gkt037. PubMed PMID: 23358822; PubMed Central PMCID: PMCPMC3597698.
12. Pefanis E, Wang J, Rothschild G, Lim J, Chao J, Rabadan R, et al. Noncoding RNA transcription targets AID to divergently transcribed loci in B cells. Nature. 2014;514(7522):389-93. Epub 2014/08/15. doi: 10.1038/nature13580. PubMed PMID: 25119026; PubMed Central PMCID: PMCPMC4372240.
13. Morton DJ, Kuiper EG, Jones SK, Leung SW, Corbett AH, Fasken MB. The RNA exosome and RNA exosome-linked disease. Rna. 2018;24(2):127-42. doi: 10.1261/rna.064626.117. PubMed PMID: WOS:000422717400001.
14. Muller JS, Giunta M, Horvath R. Exosomal Protein Deficiencies: How Abnormal RNA Metabolism Results in Childhood-Onset Neurological Diseases. J Neuromuscul Dis. 2015;2(Suppl 2):S31-S7. Epub 2015/01/01. doi: 10.3233/JND-150086. PubMed PMID: 27127732; PubMed Central PMCID: PMCPMC4845884.

15. Wan J, Yourshaw M, Mamsa H, Rudnik-Schoneborn S, Menezes MP, Hong JE, et al. Mutations in the RNA exosome component gene EXOSC3 cause pontocerebellar hypoplasia and spinal motor neuron degeneration. Nat Genet. 2012;44(6):704-8. Epub 2012/05/01. doi: 10.1038/ng.2254. PubMed PMID: 22544365; PubMed Central PMCID: PMC3366034.

16. Eggens VR, Barth PG, Niermeijer JM, Berg JN, Darin N, Dixit A, et al. EXOSC3 mutations in pontocerebellar hypoplasia type 1: novel mutations and genotype-phenotype correlations. Orphanet J Rare Dis. 2014;9(1):23. Epub 2014/02/15. doi: 10.1186/1750-1172-9-23. PubMed PMID: 24524299; PubMed Central PMCID: PMC3928094.

17. Rudnik-Schoneborn S, Senderek J, Jen JC, Houge G, Seeman P, Puchmajerova A, et al. Pontocerebellar hypoplasia type 1: clinical spectrum and relevance of EXOSC3 mutations. Neurology. 2013;80(5):438-46. Epub 2013/01/04. doi: 10.1212/WNL.0b013e31827f0f66. PubMed PMID: 23284067; PubMed Central PMCID: PMCPMC3590055.

18. Halevy A, Lerer I, Cohen R, Kornreich L, Shuper A, Gamliel M, et al. Novel EXOSC3 mutation causes complicated hereditary spastic paraplegia. J Neurol. 2014;261(11):2165-9. Epub 2014/08/26. doi: 10.1007/s00415-014-7457-x. PubMed PMID: 25149867.

19. Zanni G, Scotton C, Passarelli C, Fang M, Barresi S, Dallapiccola B, et al. Exome sequencing in a family with intellectual disability, early onset spasticity, and cerebellar atrophy detects a novel mutation in EXOSC3. Neurogenetics. 2013;14(3-4):247-50. Epub 2013/08/27. doi: 10.1007/s10048-013-0371-z. PubMed PMID: 23975261.

20. Fasken MB, Losh JS, Leung SW, Brutus S, Avin B, Vaught JC, et al. Insight into the RNA Exosome Complex Through Modeling Pontocerebellar Hypoplasia Type 1b Disease Mutations in Yeast. Genetics. 2017;205(1):221-37. Epub 2016/10/27. doi: 10.1534/genetics.116.195917. PubMed PMID: 27777260; PubMed Central PMCID: PMCPMC5223504.

21. Gillespie A, Gabunilas J, Jen JC, Chanfreau GF. Mutations of EXOSC3/Rrp40p associated with neurological diseases impact ribosomal RNA processing functions of the exosome in S. cerevisiae. RNA. 2017;23(4):466-72. Epub 2017/01/06. doi: 10.1261/rna.060004.116. PubMed PMID: 28053271; PubMed Central PMCID: PMCPMC5340910.

22. Zinder JC, Lima CD. Targeting RNA for processing or destruction by the eukaryotic RNA exosome and its cofactors. Genes Dev. 2017;31(2):88-100. Epub 2017/02/17. doi: 10.1101/gad.294769.116. PubMed PMID: 28202538; PubMed Central PMCID: PMCPMC5322736.

23. Belair C, Sim S, Kim KY, Tanaka Y, Park IH, and, et al. The RNA exosome nuclease complex regulates human embryonic stem cell differentiation. J Cell Biol. 2019. Epub 2019/07/17. doi: 10.1083/jcb.201811148. PubMed PMID: 31308215.

24. Mistry DS, Chen Y, Sen GL. Progenitor function in self-renewing human epidermis is maintained by the exosome. Cell Stem Cell. 2012;11(1):127-35. Epub 2012/07/10. doi: 10.1016/j.stem.2012.04.022. PubMed PMID: 22770246; PubMed Central PMCID: PMCPMC3392610.

25. McIver SC, Kang YA, DeVilbiss AW, O'Driscoll CA, Ouellette JN, Pope NJ, et al. The exosome complex establishes a barricade to erythroid maturation. Blood. 2014;124(14):2285-97. Epub 2014/08/15. doi: 10.1182/blood-2014-04-571083. PubMed PMID: 25115889; PubMed Central PMCID: PMCPMC4183988.

26. Kiss DL, Andrulis ED. Genome-wide analysis reveals distinct substrate specificities of Rrp6, Dis3, and core exosome subunits. RNA. 2010;16(4):781-91. Epub 2010/02/27. doi: 10.1261/rna.1906710. PubMed PMID: 20185544; PubMed Central PMCID: PMCPMC2844625.

27. Biancheri R, Cassandrini D, Pinto F, Trovato R, Di Rocco M, Mirabelli-Badenier M, et al. EXOSC3 mutations in isolated cerebellar hypoplasia and spinal anterior horn involvement. J Neurol. 2013;260(7):1866-70. Epub 2013/04/09. doi: 10.1007/s00415-013-6896-0. PubMed PMID: 23564332.

28. Di Giovambattista AP, Jacome Querejeta I, Ventura Faci P, Rodriguez Martinez G, Ramos Fuentes F. [Familial EXOSC3-related pontocerebellar hypoplasia]. An Pediatr (Barc). 2017;86(5):284-6. Epub 2016/11/24. doi: 10.1016/j.anpedi.2016.09.011. PubMed PMID: 27876572.

29. Eggens VR, Barth PG, Niermeijer JM, Berg JN, Darin N, Dixit A, et al. EXOSC3 mutations in pontocerebellar hypoplasia type 1: novel mutations and genotype-phenotype correlations. Orphanet J

Rare Dis. 2014;9:23. Epub 2014/02/15. doi: 10.1186/1750-1172-9-23. PubMed PMID: 24524299; PubMed Central PMCID: PMCPMC3928094.

30. Bizzari S, Hamzeh AR, Mohamed M, Al-Ali MT, Bastaki F. Expanded PCH1D phenotype linked to EXOSC9 mutation. Eur J Med Genet. 2019. Epub 2019/01/29. doi: 10.1016/j.ejmg.2019.01.012. PubMed PMID: 30690203.

31. Burns DT, Donkervoort S, Muller JS, Knierim E, Bharucha-Goebel D, Faqeih EA, et al. Variants in EXOSC9 Disrupt the RNA Exosome and Result in Cerebellar Atrophy with Spinal Motor Neuronopathy. Am J Hum Genet. 2018;102(5):858-73. Epub 2018/05/05. doi: 10.1016/j.ajhg.2018.03.011. PubMed PMID: 29727687; PubMed Central PMCID: PMCPMC5986733.

32. Lorentzen E, Dziembowski A, Lindner D, Seraphin B, Conti E. RNA channelling by the archaeal exosome. EMBO Rep. 2007;8(5):470-6. Epub 2007/03/24. doi: 10.1038/sj.embor.7400945. PubMed PMID: 17380186; PubMed Central PMCID: PMCPMC1866195.

33. Wasmuth EV, Zinder JC, Zattas D, Das M, Lima CD. Structure and reconstitution of yeast Mpp6-nuclear exosome complexes reveals that Mpp6 stimulates RNA decay and recruits the Mtr4 helicase. Elife. 2017;6. Epub 2017/07/26. doi: 10.7554/eLife.29062. PubMed PMID: 28742025; PubMed Central PMCID: PMCPMC5553935.

34. Zinder JC, Wasmuth EV, Lima CD. Nuclear RNA Exosome at 3.1 A Reveals Substrate Specificities, RNA Paths, and Allosteric Inhibition of Rrp44/Dis3. Mol Cell. 2016;64(4):734-45. Epub 2016/11/08. doi: 10.1016/j.molcel.2016.09.038. PubMed PMID: 27818140; PubMed Central PMCID: PMCPMC5115963.

35. Ivanov I, Atkinson D, Litvinenko I, Angelova L, Andonova S, Mumdjiev H, et al. Pontocerebellar hypoplasia type 1 for the neuropediatrician: Genotype-phenotype correlations and diagnostic guidelines based on new cases and overview of the literature. Eur J Paediatr Neurol. 2018;22(4):674-81. Epub 2018/04/17. doi: 10.1016/j.ejpn.2018.03.011. PubMed PMID: 29656927.

36. Falk S, Bonneau F, Ebert J, Kogel A, Conti E. Mpp6 Incorporation in the Nuclear Exosome Contributes to RNA Channeling through the Mtr4 Helicase. Cell Rep. 2017;20(10):2279-86. Epub 2017/09/07. doi: 10.1016/j.celrep.2017.08.033. PubMed PMID: 28877463; PubMed Central PMCID: PMCPMC5603729.

37. Schwabova J, Brozkova DS, Petrak B, Mojzisova M, Pavlickova K, Haberlova J, et al. Homozygous EXOSC3 mutation c.92G-->C, p.G31A is a founder mutation causing severe pontocerebellar hypoplasia type 1 among the Czech Roma. J Neurogenet. 2013;27(4):163-9. Epub 2013/07/26. doi: 10.3109/01677063.2013.814651. PubMed PMID: 23883322.

38. Gratz SJ, Wildonger J, Harrison MM, O'Connor-Giles KM. CRISPR/Cas9-mediated genome engineering and the promise of designer flies on demand. Fly (Austin). 2013;7(4):249-55. Epub 2013/10/04. doi: 10.4161/fly.26566. PubMed PMID: 24088745; PubMed Central PMCID: PMCPMC3896497.

39. Gratz SJ, Ukken FP, Rubinstein CD, Thiede G, Donohue LK, Cummings AM, et al. Highly specific and efficient CRISPR/Cas9-catalyzed homology-directed repair in Drosophila. Genetics. 2014;196(4):961-71. Epub 2014/01/31. doi: 10.1534/genetics.113.160713. PubMed PMID: 24478335; PubMed Central PMCID: PMCPMC3982687.

40. Bauer JH, Goupil S, Garber GB, Helfand SL. An accelerated assay for the identification of lifespan-extending interventions in Drosophila melanogaster. Proc Natl Acad Sci U S A. 2004;101(35):12980-5. Epub 2004/08/26. doi: 10.1073/pnas.0403493101. PubMed PMID: 15328413; PubMed Central PMCID: PMCPMC516504.

41. Pak C, Garshasbi M, Kahrizi K, Gross C, Apponi LH, Noto JJ, et al. Mutation of the conserved polyadenosine RNA binding protein, ZC3H14/dNab2, impairs neural function in Drosophila and humans. Proc Natl Acad Sci U S A. 2011;108(30):12390-5. Epub 2011/07/08. doi: 10.1073/pnas.1107103108. PubMed PMID: 21734151; PubMed Central PMCID: PMCPMC3145741.

Figure Legends

Fig 1: The Rrp40 subunit of the RNA exosome is required for viability in *Drosophila* and for an age-dependent function in neurons. (A) The RNA exosome is an evolutionarily conserved ribonuclease complex composed of nine structural subunits termed exosome components (EXOSC1-9)—three Cap subunits: EXOSC1; EXOSC2; EXOSC3, six Core Ring subunits: EXOSC4 (not visible); EXOSC5; EXOSC6; EXOSC7 (not visible); EXOSC8; EXOSC9, and a Catalytic Base subunit: Dis3. Mutations in the *EXOSC3* gene encoding a cap subunit [light blue, labeled with 3 (termed Rrp40 in *Drosophila*)] cause PCH1b [5]. (B) Tissue-specific drivers as indicated were employed to knockdown Rrp40 in *Drosophila*. The percentage of flies eclosed (of expected) for the indicated genotypes is shown for a total of 300 flies for each genotype. (C) A scheme to illustrate the approach to achieve temperature-sensitive knockdown of Rrp40 is shown: The *Gal80^{ts}* allele shifts between 18°C (blue, RNAi off) and 29°C (red, RNAi on). E0=0hr embryo, L1/2/3=1st, 2nd or 3rd instar larvae; WPP=white prepupa. (D) The viability of flies in which temperature sensitive RNAi (C) was employed to deplete Rrp40 24 hours post egg laying is shown. The viability of these post-embryonic RNAi survivors as percentage of flies eclosed (of expected) is shown for the indicated tissue-specific drivers. (E) Kaplan-Meier analysis of post-embryonic RNAi survivors for either control (*Gal4* alone) or temperature sensitive knockdown (*tub> Gal80^{ts}*) for the following tissue-specific drivers: Neuronal (*elav>Gal4*, n=50); Muscle (*Mhc>Gal4*, n=50); or Glial *(repo>Gal4*, n=50*)*.

Fig 2: Generation of *Drosophila* model of PCH1b amino acid substitutions. (A) The EXOSC3/Rrp40 protein consists of three domains: an N-terminal domain (N), a central S1 putative RNA binding domain, and a C-terminal putative RNA binding KH (K homology) domain. The disease-causing amino acid substitutions (G31A and D132A) modeled in *Drosophila* in this study are indicated in red above the domain structure. The position and flanking sequence of the amino acid substitutions in PCH1b-associated human EXOSC3 (shown in red) and the corresponding amino acids in *Mus musculus* (*Mm*), *Drosophila melanogaster* (*Dm*), and *Saccharomyces cerevisiae* (*Sc*) are shown. (B) The amino acid substitutions that occur in EXOSC3 in patients, which are modeled in *Drosophila* Rrp40, are indicated with Patient Genotype (Homozygous/Heterozygous) as modeled in *Drosophila* (*Drosophila* Genotype) shown. For each *Drosophila* model, the viability of that genotype engineered in flies by CRISPR/Cas9 gene editing is shown as % eclosed (of expected). *Rrp40* mutants show decreased viability, indicated by skewed Mendelian ratios. n= the number of individual flies analyzed. (C) A Kaplan-Meier

analysis shows that *Rrp40* mutant flies with the indicated genotypes that model patient genotypes exhibit early adult lethality compared to wild-type Control flies (w^{1118}) or *Rrp40-WT* ($Rrp40^{wt}$) flies that have undergone CRISPR/Cas9 gene editing to produce a control wild-type *Rrp40* allele (see Materials and methods).

Fig 3: Flies that model PCH1b amino acid substitutions in *Drosophila* show a range of morphological and behavioral phenotypes. (A) *Rrp40* mutant flies show a progressive wing position phenotype in adults. Abnormal wing posture phenotypes (wings held-up or -out) are shown for *Rrp40* mutant flies compared to *Rrp40-WT* flies. (B) Quantitative analysis of the abnormal wing position phenotype of *Rrp40* mutants raised at 25°C. The percentages of adults with abnormal wing position over time (Days post-eclosion) were calculated based on 60 flies per genotype. Neither w^{1118} nor Control *Rrp40-WT* flies showed any abnormal wing position (0% abnormal wing posture, n>100) over the time course analyzed. (C) Locomotor activity was assessed using a negative geotaxis assay as described in Materials and methods. Data are presented as the average percentage of flies of the indicated genotypes that reach the top of a cylinder after 60 seconds across all trials. Groups of 10 age-matched flies [Day (1) and Day (6)] were tested for at least three independent trials per genotype. Values represent the mean ± SEM for n= 3 independent experiments. Asterisks (*) indicate results that are statistically significance at *P-value < 0.05.

Fig 4: Locomotor defects in *Rrp40* mutant flies are rescued by neuronal expression of human *EXOSC3*. (A) Transgenic flies that express human *EXOSC3* under a UAS were generated as described in Materials and methods. The percentage of flies eclosed (of expected) for the indicated genotypes which includes flies with transgenic *EXOSC3*, but no driver (rescue control) or flies with the UAS and a pan-neuronal driver (*elav*) (pan-neuronal rescue) is indicated. (B) Locomotor assays were employed to assess whether expression of human *EXOSC3* rescues behavioral phenotypes in *Rrp40* mutant flies. Data are presented as the average percentage of flies that reach the top of a cylinder after 60 seconds across all trials. Groups of 10 age-matched flies (Day 6) were tested for at least 3 independent trials per genotype. Results are shown for control *Rrp40-WT* flies as compared to either $Rrp40^{G11A}$ (G11A/G11A, left) or $Rrp40^{D87A}$ (D87A/D87A, right) homozygous flies that either do not express human *EXOSC3* (-) or do express human *EXOSC3* (+*Gal4*). Values represent the mean ± SEM for n= 3 independent experiments. Asterisks (*) indicate results that are statistical significance at *P-value < 0.05.

Fig 5: Amino acid substitutions that model PCH1b in Rrp40 do not grossly affect the levels of Rrp40 or other RNA exosome subunits. (A) Lysates prepared from control *Rrp40-WT* or *Rrp40* mutant whole flies were resolved by SDS-PAGE and analyzed by immunoblotting with RNA exosome cap subunits antibodies (Rrp40/EXOSC3, Rrp4/EXOSC2 or Csl4/EXOSC1) or a core ring subunit (Mtr3/EXOSC6). (B) Lysate prepared from heads of control *Rrp40*^{wt} or *Rrp40* mutant flies were resolved by SDS-PAGE and analyzed by immunoblotting with antibodies described above. Both LaminD and Stain Free, as a measure of total protein loaded, serve as loading controls. Representative experiments from two independent immunoblots are shown.

Fig 6: RNA-seq analysis of *Rrp40* mutant flies reveals distinct transcriptomes. (A) Principal component analysis (PCA) analysis of RNA-seq data from adult *Drosophila* heads from *Rrp40-WT* and *Rrp40* mutant flies (*Rrp40*^{G11A} and *Rrp40*^{D87A}) shows that results from the three independent experiments cluster based on the genotype and that mutants are distinct from one another and from control flies. (B,C) Volcano plots show transcripts differentially expressed in both *Rrp40* mutants [(B) *G11A/G11A* (2,368) and (C) *D87A/D87A* (3,511)] compared to *Rrp40*-WT (FDR $p<0.05$, DEseq). The number of transcripts that show ≥ 5-fold change in steady-state levels (Down or Up) are indicated to the side in each plot. Representative regulators of neuronal function in flies are highlighted. (D) A Venn diagram illustrates the fraction of protein-coding (mRNA) and non-coding (ncRNA) transcripts changed 5-fold or more that are common to the *Rrp40* mutant flies. (E) A pie chart shows the distribution of differentially expressed genes, by evaluating the percentage of total RNAs increased at least 5-fold in each *Rrp40* mutant corresponding to mRNA or non-coding RNA. (F) A pie chart illustrates the classes of ncRNAs increased at least 5-fold in each *Rrp40* mutant (lncRNAs, long noncoding RNAs; asRNAs, Antisense RNAs; tRNAs, transfer RNAs; snoRNAs, small nucleolar RNAs; sisRNAs, stable intronic sequence RNAs; scaRNAs, small Cajal body RNAs). (G) The top 10 significant (Adj. P-val < 0.05) pathways from Gene Ontology (GO) molecular function categories from FlyEnrichr database base. GO term analysis was performed on transcripts that are increased in each *Rrp40* mutant (left, *G11A/G11A*; right, *D87A/D87A*) as compared to *Rrp40-WT*.

Fig 7: Key neuronal transcripts show an increase in steady-state levels in *Rrp40* mutant flies. (A) An Integrative Genomic View (IGV) screenshot (http://software.broadinstitute.org/software/igv/) of *Arc1* track peaks across the *Drosophila* genome (dm6 assembly) in *Rrp40* mutants [*Rrp40 D87A/D87A* (Upper) and *Rrp40 G11A/G11A* (Middle)] as well as *Rrp40-WT* (WT, Lower). Chromosome number and location (red rectangle; top) are displayed at the top. (B,C) Changes in the level of representative transcripts were validated using RT-qPCR in *Rrp40-WT* and *Rrp40* mutant flies. Data are presented as the Fold Change Normalized to *Act5c* transcript (which was unchanged in the RNA-Seq datasets) where the value for the *Rrp40-WT* sample is set to 1.0. Results are presented as mean ± standard error of the mean (*P<0.05 vs. the WT group in a two-tailed *t*-test). (D) Expression of human *EXOSC3 (UAS-EXOSC3-myc)* in neurons rescues the increased steady-state levels of the *Arc1* (left) and *WFS1* (right) transcripts in both *Rrp40* mutants. The steady-state levels of the *Arc1* and *WFS1* transcripts were analyzed using RT-qPCR in control Rrp40-WT flies (set to 1.0) and mutant flies expressing human *EXOSC3* (+*Gal4*) or not (-). Data are presented as the means ± standard error of the mean (*P<0.05 vs. the WT group in a two-tailed *t*-test).

Figure 1

Morton *et al*

A

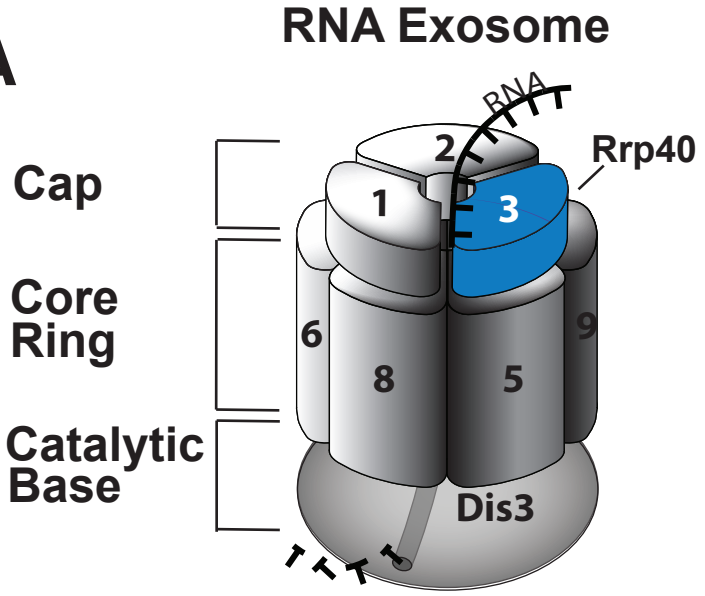

B

Viability of tissue-specifc RNAi

Genotype (+*Rrp40*^{IR})	% eclosed (of expected)
global depletion *Actin5c>Gal4*	0% n=300
neuronal depletion *elav>Gal4*	0% n=300
glial depletion *repo>Gal4*	0% n=300
muscle depletion *Mhc>Gal4*	0% n=300

C

Temperature-sensitive knockdown of *Rrp40* (*Rrp40*^{IR}; *tub>Gal80*^{ts})

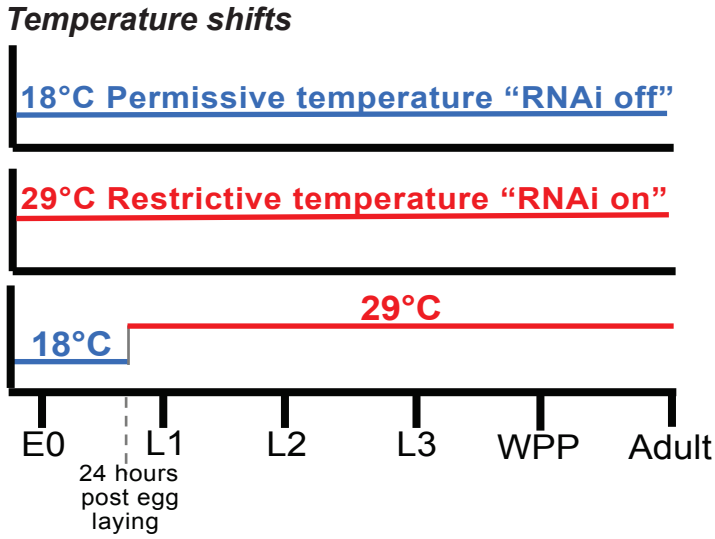

D

Frequency of post-embryonic RNAi Survivors

Genotype (+*Rrp40*^{IR}; *tub>Gal80*^{ts})	% eclosed (of expected)
global depletion *Actin5c>Gal4*	0% n=300
neuronal depletion *elav>Gal4*	6% n=300
glial depletion *repo>Gal4*	1% n=300
muscle depletion *Mhc>Gal4*	63% n=300

E

Lifespan of post-embryonic RNAi Survivors

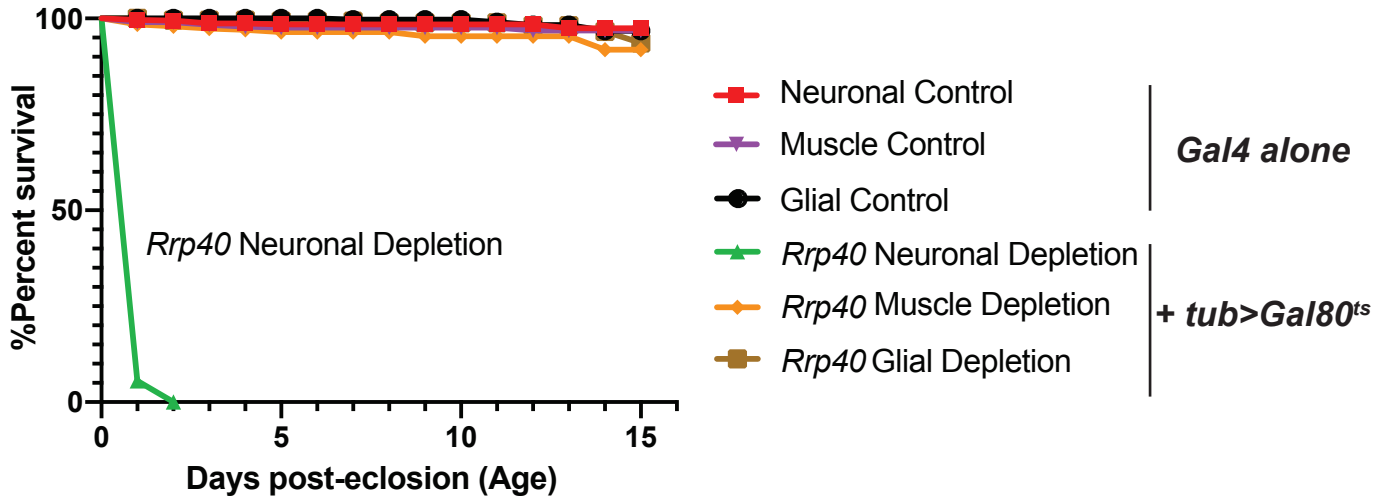

A

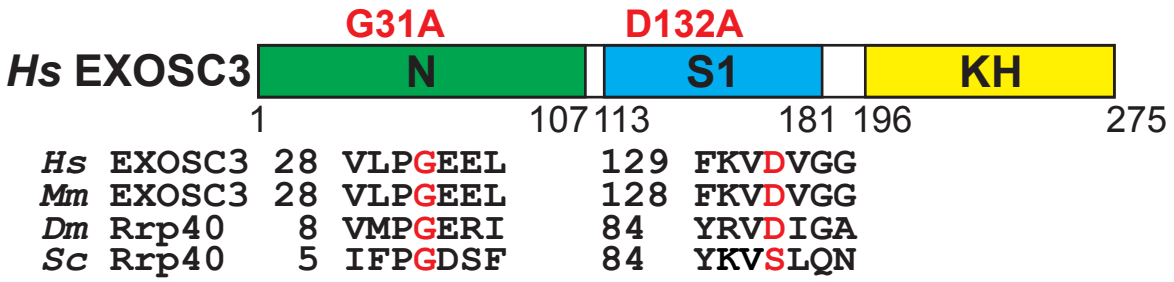

B

EXOSC3	Rrp40	Patient Genotype	*Drosophila* Genotype	% eclosed (of expected)
G31A	*G11A*	*G31A* Homozygous	*G11A* Homozygous	14% n=126
D132A	*D87A*	*D132A* Homozygous	*D87A* Homozygous	38% n=182
		D132A/null Heterozygous	*D87A/Df(2L)* Heterozygous	15% n=160

C

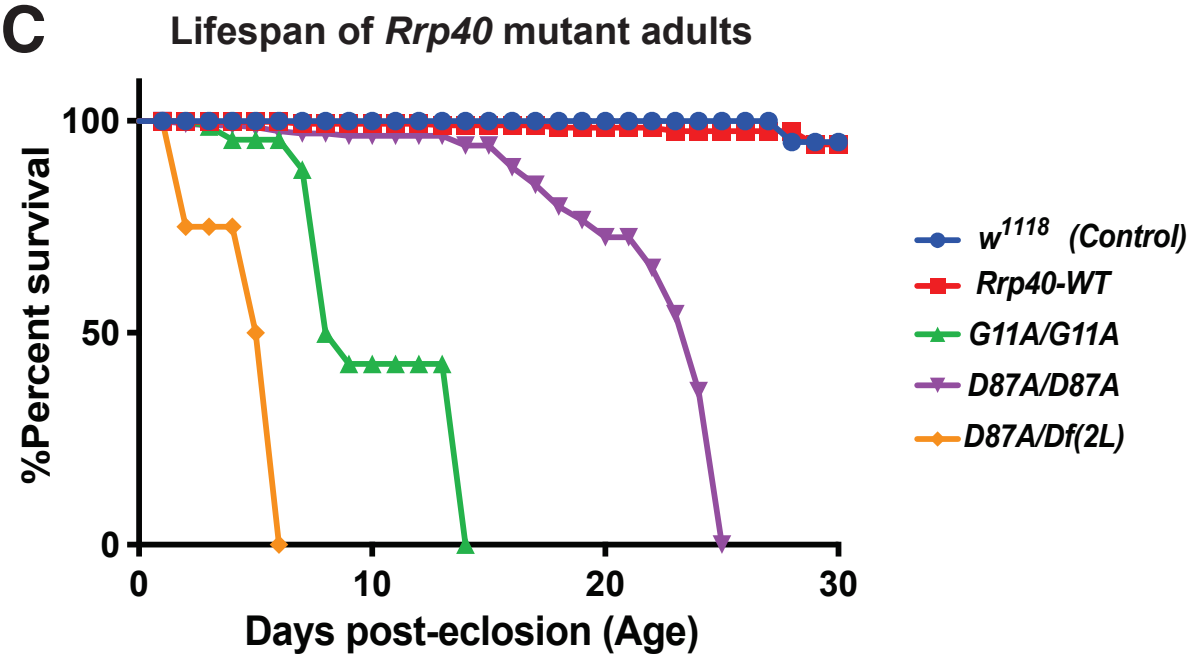

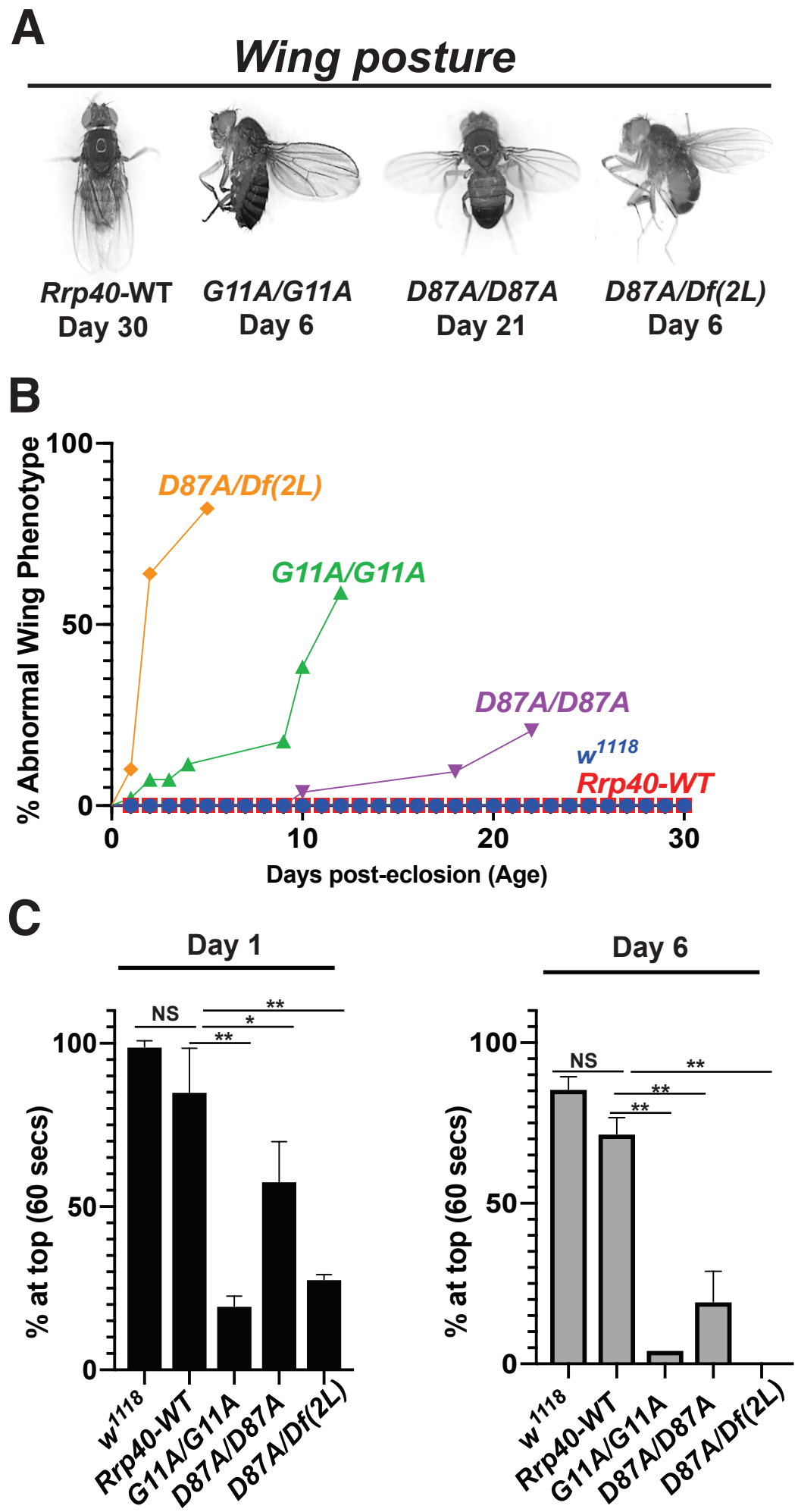
A
Wing posture
Rrp40-WT
Day 30
G11A/G11A
Day 6
D87A/D87A
Day 21
D87A/Df(2L)
Day 6
B
% Abnormal Wing Phenotype
100
50
0
D87A/Df(2L)
G11A/G11A
D87A/D87A
w1118
Rrp40-WT
0
10
20
30
Days post-eclosion (Age)
C
Day 1
Day 6
% at top (60 secs)
NS
**
*
w1118
Rrp40-WT
G11A/G11A
D87A/D87A
D87A/Df(2L)

Figure 4

A

Genotype	% eclosed (of expected)
Rrp40^{wt}/*Rrp40*^{wt}	93% n=52
Rrp40^{G11A}/*Rrp40*^{G11A}; *UAS-EXOSC3-myc* (rescue control)	22% n=63
elav-Gal4>Rrp40^{G11A}/*Rrp40*^{G11A};*UAS-EXOSC3-myc* (pan-neuronal rescue)	20% n=87
Rrp40^{D87A}/*Rrp40*^{D87A}; *UAS-EXOSC3-myc* (rescue control)	37% n=79
elav-Gal4>Rrp40^{D87A}/*Rrp40*^{D87A};*UAS-EXOSC3-myc* (pan-neuronal rescue)	40% n=124

B

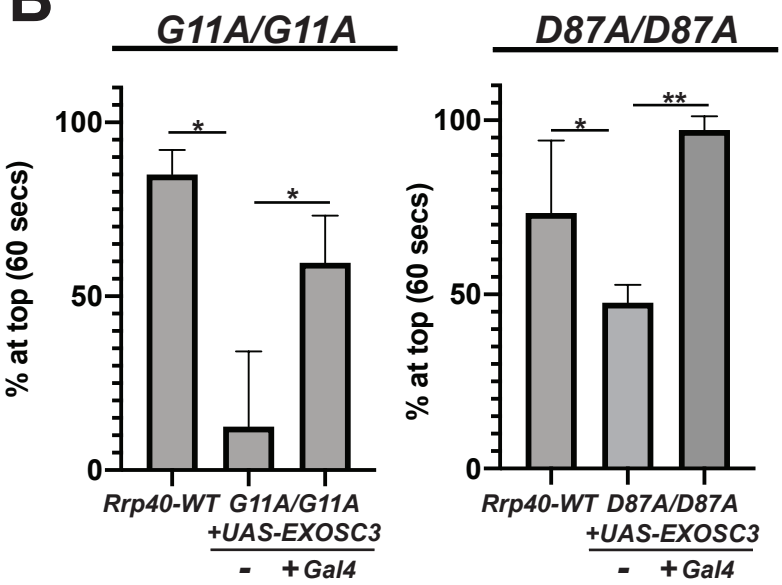

Figure 5

Morton *et al*

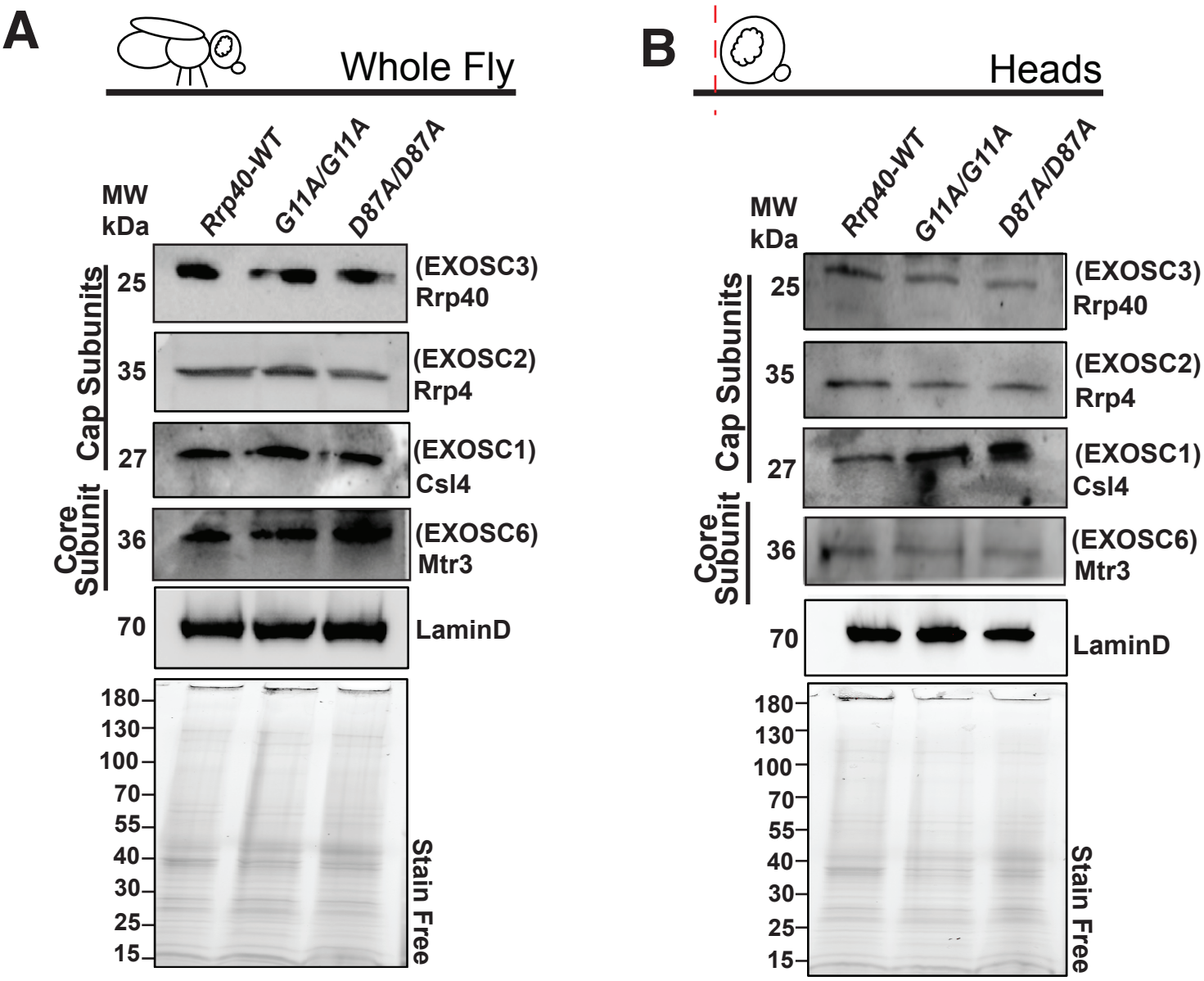

Figure 6

Morton *et al*

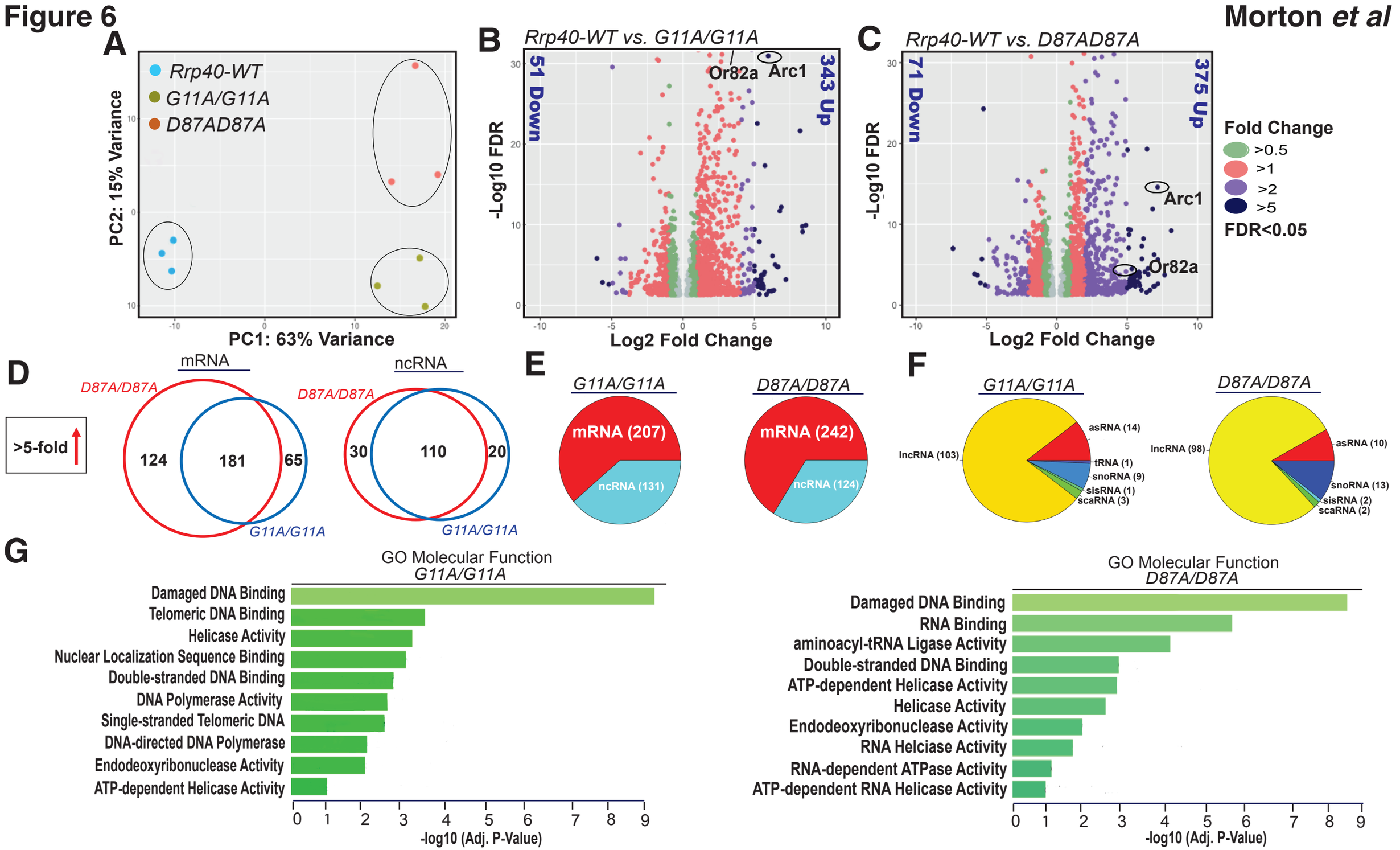

Figure 7

Morton *et al*

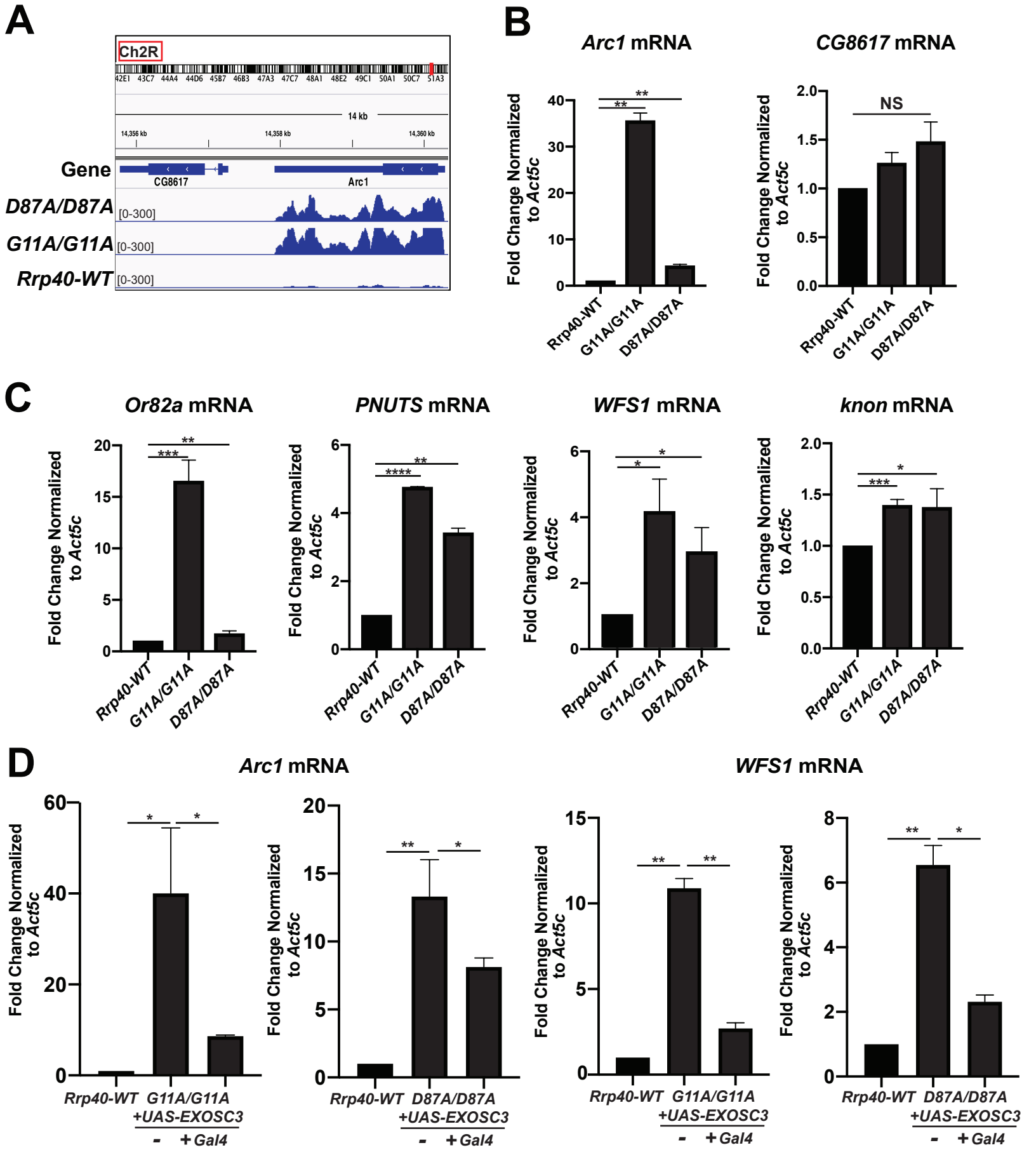

Figure Legends for Supporting Information

S1 Fig: CRISPR/Cas9-induced Homology-directed recombination (HDR) with a double-stranded DNA donor vector. (A) Schematic of the HDR strategy used to replace the *Rrp40* locus with the *Rrp40-3xP3-DsRed* vector, which drives expression of DsRed in the eye. The DsRed is flanked by loxP recombination sites to remove DsRed if desired. The guide RNA (gRNA) target site is indicated (red arrow). Homology arms of 1kb immediately flanking *Rrp40* were cloned into the *Rrp40-3xP3-DsRed* vector.

S2 Fig: *EXOSC3*-PCH1b mutations modeled in *Drosophila Rrp40*. (A,B) Sequences confirming the creation of CRISPR/Cas9 genome-edited flies $Rrp40^{D87A}$ (A) and $Rrp40^{G11A}$ (B) isolates are shown. The engineered mutations in the *Rrp40* locus are highlighted in red and are noted along with sequencing traces of $Rrp40^{D87A}$ (C) and $Rrp40^{G11A}$ (D) confirming the edited alleles.

S3 Fig: PCH1b-linked *Rrp40* mutant alleles function as hypomorphs. (A) A summary of the viability of $Rrp40^{G11A}$ or $Rrp40^{D87A}$ over a genomic deletion *Df(2L) Exel600*, percentage of flies eclosed (of expected) for indicated genotypes.

S4 Fig: Expression Profiles of *Rrp40* mutants are distinct. (A) A volcano plot shows transcripts differentially expressed in the *Rrp40* mutants: $Rrp40^{G11A}$-Up: (181) and $Rrp40^{D87A}$-Up: (143) compared to one another ($q<0.05$, >1-fold change). (B) Pie chart showing the distribution of differentially expressed genes, by evaluating the percentage of mRNAs and ncRNAs (lncRNAs, long noncoding RNAs; asRNAs, anti-sense RNAs)that increase in each *Rrp40* mutant compared to one another.

S5 Fig: Integrative Genomic View (IGV) screenshots of multiple functionally important neuronal to illustrate the RNA-Seq data obtained. Integrative Genomics Viewer screenshot (http://software.broadinstitute.org/software/igv/) of *WFS1* (A), *Or82a* (B), *PNUTS* (C) and *knon (CG7813)* track peaks across the *Drosophila* genome (dm6 assembly) in *Rrp40* mutants [$Rrp40^{G11A}$ (Middle) and $Rrp40^{D87A}$ (Upper)] as well as $Rrp40^{wt}$ (WT, lower).

S1 Table: Oligonucleotide Primer Sequences employed for RT-qPCR.

S2-4 Tables: RNA-Seq data analysis of *Rrp40* alleles.

S1 Video: Negative geotaxis assays for (A) $Rrp40^{wt}$, (B) $Rrp40^{G11A}$, and (C) $Rrp40^{D87A}$ at day 4.

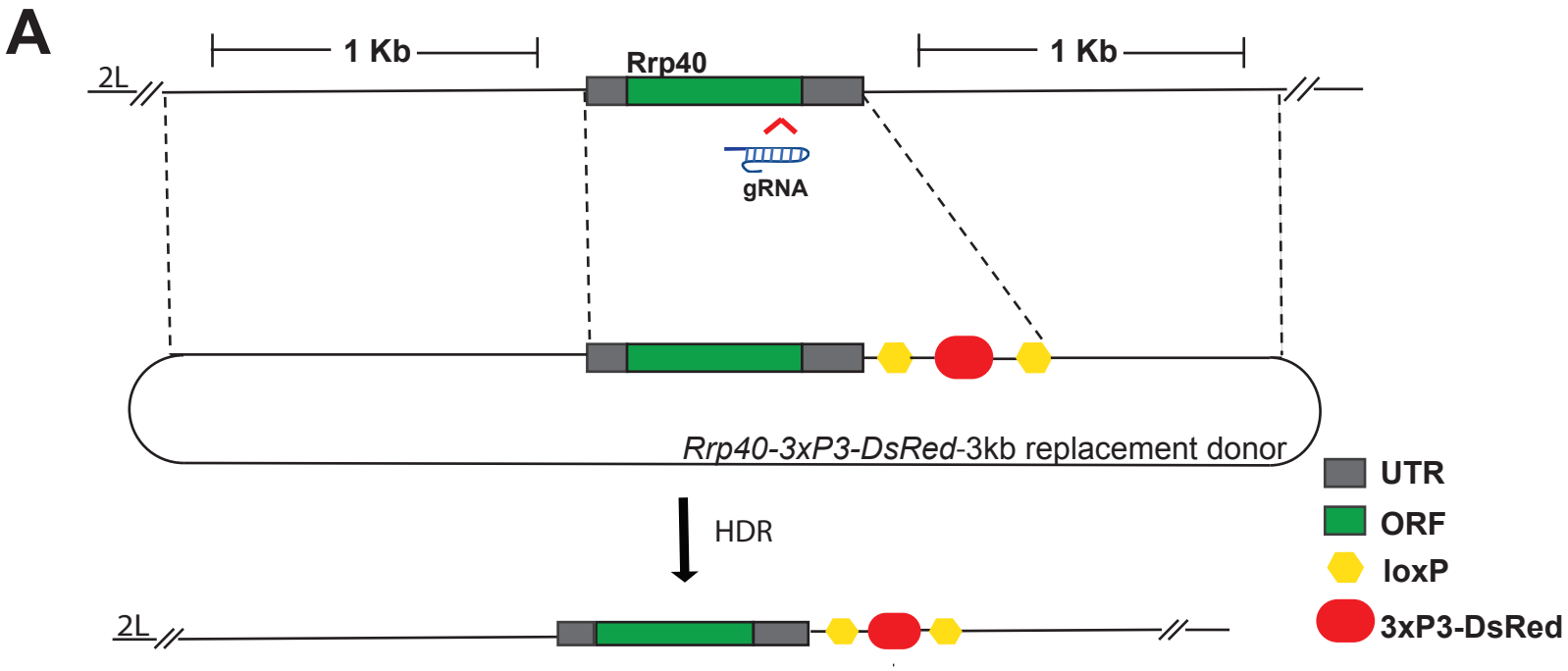
A
1 Kb
1 Kb
2L
Rrp40
gRNA
Rrp40-3xP3-DsRed-3kb replacement donor
HDR
2L
UTR
ORF
loxP
3xP3-DsRed

S2 Figure

Morton *et al*

A

```
>D87Aseq_1_Rrp40F_A10
ATGAGCGCGACCAGCACAATAGTTATGCCCGGTGAGCGAATTGCGGCCATTGAGGAGCTGGCGAAGAGCA
AGCGGGTGATACTCGGACCGGGACTGCGGCGTCTGGATGACACGGTGGTGGCCAGCAAGGCAGGCCCACT
TCGACACAAGGAACCCGGCACCTTCTGGGTGGACAACTACCAGAGGAGGTACATCCCGGCACGCGGGGAT
CTCATTCTGGGCATTGTGCGAGCCAAGGCGGGCGATCTGTACCGCGTGGCCATTGGAGCAACGGACACAG
CCTCCATATCGTATCTCGCCTTTGAGGCGGCCACCAAGAAGAATCGCCCGGATCTGATCCCCGGTGATCT
GATTTATGCGAGAGTCCTGAATGCCAGCGCGGACATTGAACCGGAGCTGGTCTGCGTCAACTCGGTGGGC
AAAAGTGGCAAACTGGGCGTCCTCACCGATGGATTCTTCTTCAAGTGCAGCCTGAATCTGGGAAGGATGC
TGCTGCGGGAAAACTGCCCTGTTCTCGCCGCTCTTACCCGGGAACTGCCCTACGAGATCGCTGTGGGAGT
CAACGGCAGGATATGGTTGAAGGCCCATTCCCTGACCGTGGCCCTCGCCAATGCCATTTCAGCGCTGGAG
CAATCGGGATGTGCGGAAATCGACAAAATATGTGGCAATCTCGGAGACTTCCTGCAGGCCTAG
```

B

```
>G11Aseq_4_Rrp40-F_H02
GGAGTTTCAAATCGTAAAAGCAACATTAAAATGAGCGCGACCAGCACAATAGTTATGCCCGCTGAGCGAA
TTGCGGCCATTGAGGAGCTGGCGAAGAGCAAGCGGGTGATACTCGGACCGGGACTGCGGCGTCTGGATGA
CACGGTGGTGGCCAGCAAGGCAGGCCCACTTCGACACAAGGAACCCGGCACCTTCTGGGTGGACAACTAC
CAGAGGAGGTACATCCCGGCACGCGGGGATCTCATTCTGGGCATTGTGCGAGCCAAGGCGGGCGATCTGT
ACCGCGTGGACATCGGAGCAACGGACACAGCCTCCATATCGTATCTCGCCTTTGAGGCGGCCAGCAAGAA
GAATCGCCCGGATCTGATCCCCGGTGATCTGATTTACGCGAGAGTCCTGAATGCAAGCGCGGACATTGAA
CCGGAGCTGGTCTGCGTCAACTCGGTGGGCAAAAGTGGCAAACTGGGCGTCCTCACCGATGGATTCTTCT
TCAAGTGCAGCCTGAATCTGGGAAGGATGCTGCTGCGGGAAAACTGCCCTGTTCTCGCCGCTCTTACCCG
GGAACTGCCCTACGAGATCGCTGTGGGAGTCAACGGCAGGATATGGTTGAAGGCCCATTCCCTGA
```

C

Rrp40^{D87A}

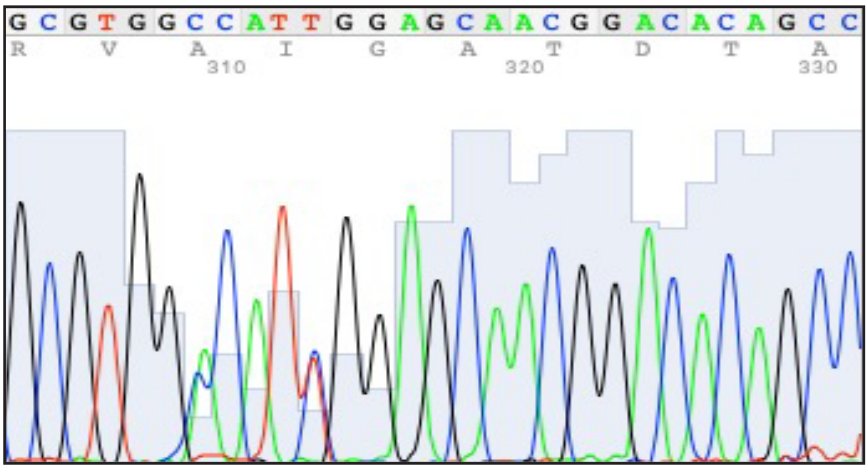

D

Rrp40^{G11A}

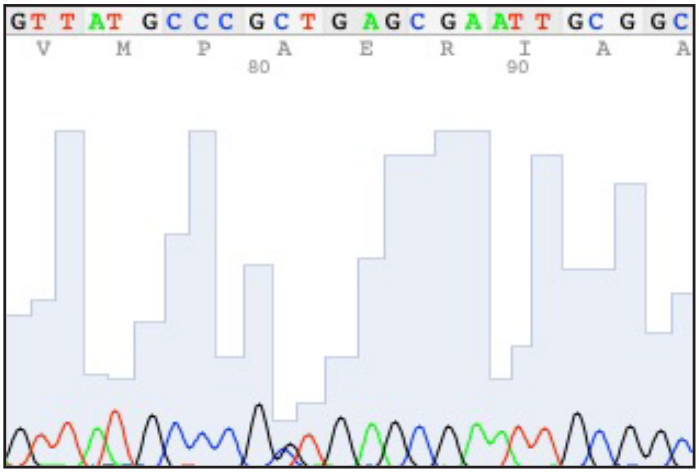

S3 Figure

Morton *et al*

EXOSC3	Rrp40	Patient Genotype	*Drosophila* Genotype	% eclosed (of expected)
G31A	G11A	G31A Homozygous	G11A Homozygous	14% n=126
		No Reported PCH1b Patient	G11A/Df(2L) Homozygous	0% n=70
D132A	D87A	D132A Homozygous	D87A Homozygous	38% n=182
		D132A/null Heterozygous	D87A/Df(2L) Heterozygous	15% n=160

S4 Figure

Morton *et al*

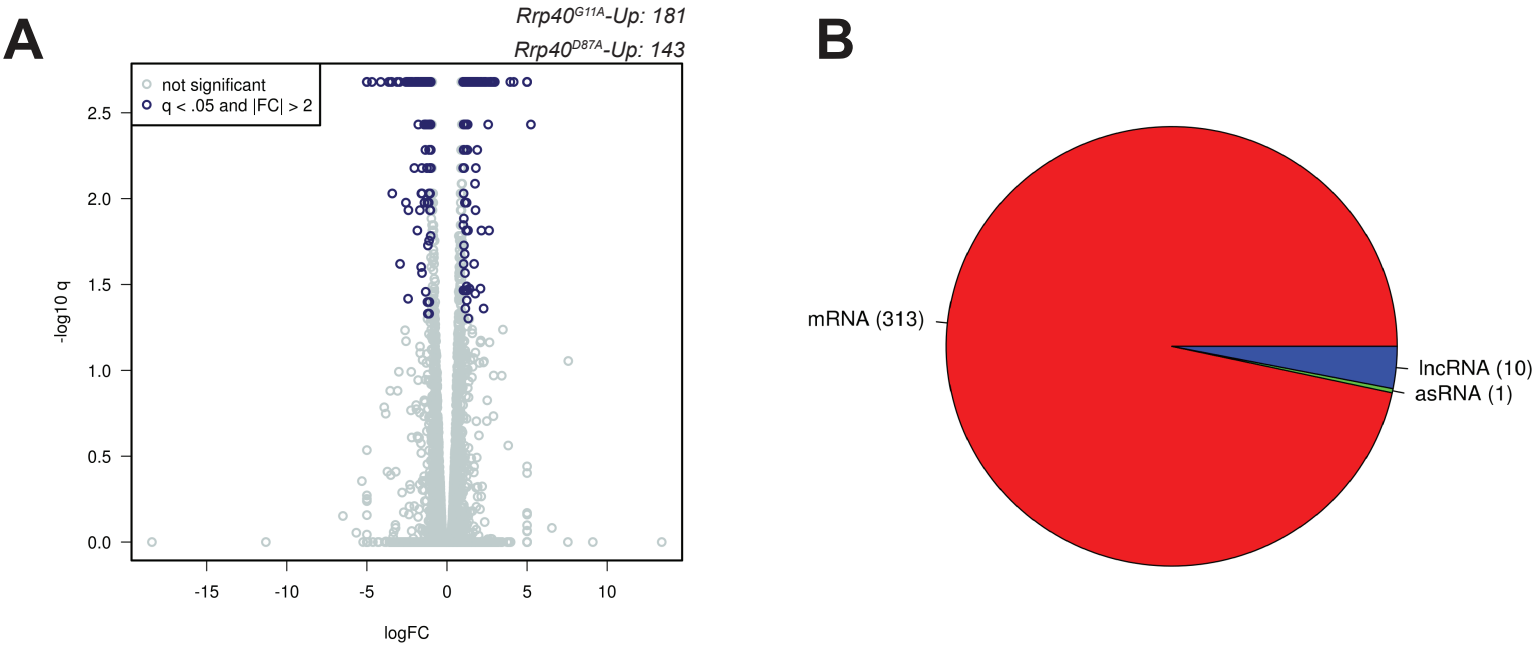

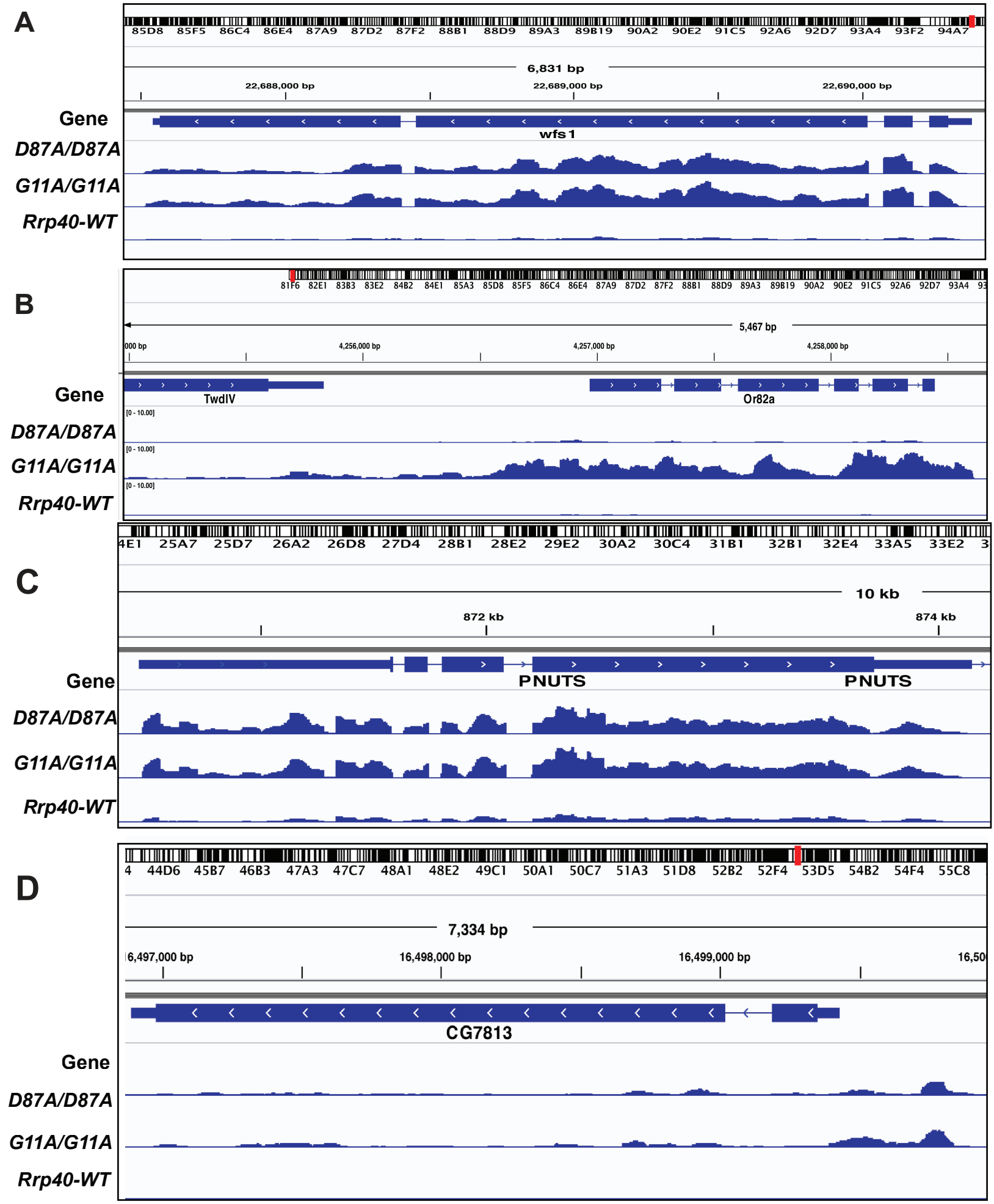
A
85D8 85F5 86C4 86E4 87A9 87D2 87F2 88B1 88D9 89A3 89B19 90A2 90E2 91C5 92A6 92D7 93A4 93F2 94A7
6,831 bp
22,688,000 bp
22,689,000 bp
22,690,000 bp
Gene
wfs1
D87A/D87A
G11A/G11A
Rrp40-WT
B
81F6 82E1 83B3 83E2 84B2 84E1 85A3 85D8 85F5 86C4 86E4 87A9 87D2 87F2 88B1 88D9 89A3 89B19 90A2 90E2 91C5 92A6 92D7 93A4
5,467 bp
4,256,000 bp
4,257,000 bp
4,258,000 bp
Gene
TwdIV
Or82a
[0 - 10.00]
D87A/D87A
[0 - 10.00]
G11A/G11A
[0 - 10.00]
Rrp40-WT
C
25A7 25D7 26A2 26D8 27D4 28B1 28E2 29E2 30A2 30C4 31B1 32B1 32E4 33A5 33E2
10 kb
872 kb
874 kb
Gene
PNUTS
PNUTS
D87A/D87A
G11A/G11A
Rrp40-WT
D
44D6 45B7 46B3 47A3 47C7 48A1 48E2 49C1 50A1 50C7 51A3 51D8 52B2 52F4 53D5 54B2 54F4 55C8
7,334 bp
6,497,000 bp
16,498,000 bp
16,499,000 bp
CG7813
Gene
D87A/D87A
G11A/G11A
Rrp40-WT

Primer Sets used in RT-qPCR

Primer Name	Primer Sequence
Arc1	FWD: GCCACAAGCACAGCAATAG REV: ATTTTTTAGCAGTTCCACGCAAC
Or82a	FWD: GCCACAAGCACAGCAATAG REV: ATTTTTAGCAGTTCCACGCAAC
WFS1	FWD: GCTCTCACATTATCCGTCCC REV: ACACAATCAAGTTAAGCAGCC
PNUTS	FWD: GACGTACCAGTCCAAATTCAG REV: GCCATTAAAGCGGGTGAAG
knon	FWD: ACCGCGTTCGTAAGTATCC REV: TCACCACCTTCTTTTCTTCATC
Act5c	FWD: GAGCGCGGTTACTCTTTCAC REV: ACTTCTCCAACGAGGAGCTG